Chinese Chemical Letters 37 (2026) 111604

Contents lists available at ScienceDirect

Chinese Chemical Letters

journal homepage: www.elsevier.com/locate/cclet

Recent advances in photocatalytic overall production of hydrogen peroxide from metal-free photocatalysts

Congxu Wang[a,c,1], Xuan Xie[d,1], Feng Qiu[a,*], Lei Zhu[b,*], Imran Shakir[e,*], Yuxi Xu[c,*]

[a] School of Physics and Optoelectronic Engineering, Hangzhou Institute for Advanced Study, University of Chinese Academy of Sciences, Hangzhou 310024, China
[b] School of Chemistry and Materials Science, Hubei Engineering Research Center for Key Technologies in Modern Paper and Sanitary Products Manufacturing, Hubei Engineering University, Xiaogan 432000, China
[c] School of Engineering, Westlake University, Hangzhou 310024, China
[d] School of Chemistry and Chemical Engineering, Northwest Normal University, Lanzhou 730070, China
[e] Department of Physics, Faculty of Science, Sustainability Research Center, Islamic University of Madinah, Madinah 42351, Saudi Arabia

ARTICLE INFO

Article history:
Received 22 May 2025
Revised 10 July 2025
Accepted 17 July 2025
Available online 17 July 2025

Keywords:
Photocatalysis
H_2O_2 generation
Metal-free photocatalysts
Tunable functionality
Overall synthesis

ABSTRACT

Hydrogen peroxide (H_2O_2) has been recognized as a green and nonpolluting multifunctional oxidant with extensive applications in environmental protection, metal etching, textile printing and dyeing, chemical synthesis and food processing. However, over 90% of industrial H_2O_2 is currently produced through the multi-step anthraquinone oxidation process, which suffers from a process with some drawbacks such as complex, high-energy consumption, and toxic byproducts emissions. Compared to the traditional anthraquinone method, artificial photosynthesis of H_2O_2 using semiconductor photocatalysts has emerged as a sustainable alternative due to its use of water and O_2 as the clean reactants and sole energy as the driving force. In recent years, metal-free photocatalysts mainly including covalent organic frameworks (COFs), covalent triazine frameworks (CTFs) and carbon nitrile (g-C_3N_4) have garnered significant interest due to their superior thermal and chemical stability, diverse synthesis methods, tunable functionality, light weight nature and non-toxicity. These materials also exhibit adjustable band structure and unique photoelectric properties. Sustainable efforts have been made to advance metal-free photocatalysts for artificial photosynthesis of H_2O_2, however, a comprehensive summary of current research status on metal-free-based photocatalytic overall H_2O_2 production remain scarce. This review outlines recent process in overall H_2O_2 photosynthesis based on metal-free photocatalysts. First, we introduced the fundamental concepts of photocatalytic overall H_2O_2 production. Then, we analyze representative studies on photocatalytic overall H_2O_2 synthesis using metal-free materials. Finally, we discuss the challenges and future perspectives in this field to guide the design and synthesis of metal-free systems for H_2O_2 generation.

© 2025 Published by Elsevier B.V. on behalf of Chinese Chemical Society and Institute of Materia Medica, Chinese Academy of Medical Sciences.

1. Introduction

The increasing of the global energy crisis and environmental pollution issues caused by excessive consumption of fossil fuel necessitate the development of low-carbon and clean energy technologies [1–8]. Hydrogen peroxide (H_2O_2) has gained much attention as a promising candidate to address these issues due to its green, environmentally friendly and sustainable nature [9–12]. H_2O_2 is irreplaceable in water treatment applications as it is a clean oxidant that decomposes into water and oxygen without producing harmful byproducts. Additionally, H_2O_2 is widely used in chemical synthesis, medicine, semiconductor manufacturing, the military, aerospace and other industries [13–15]. Moreover, it has been proposed an alternative energy carrier in fuel cells due to its safety and comparable power density as compressed hydrogen. Currently, over 90% of industrial H_2O_2 is produced *via* the traditional industrial anthraquinone (AQ) method [16,17]. However, this process involves multiples steps-hydrogenation, oxidation, extraction, purification and concentration-resulting in significant energy loss and the generation of toxic byproducts [18–20]. Furthermore, AQ method relies on precious metals catalysts, increasing the production costs. Therefore, developing an efficient, safe, green, and sustainable method for H_2O_2 preparation is an urgent task. Semiconductor based photocatalytic technology emerged as an economically viable method for utilizing solar energy to synthesize H_2O_2

* Corresponding authors.
E-mail addresses: drfqiu@ucas.edu.cn (F. Qiu), Lei.zhu@hbeu.edu.cn (L. Zhu), mshakir@iu.edu.sa (I. Shakir), xuyuxi@westlake.edu.cn (Y. Xu).
[1] These authors contributed equally in this work.

https://doi.org/10.1016/j.cclet.2025.111604
1001-8417/© 2025 Published by Elsevier B.V. on behalf of Chinese Chemical Society and Institute of Materia Medica, Chinese Academy of Medical Sciences.

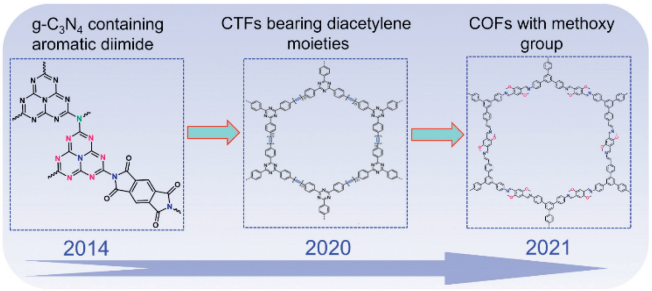


Fig. 1. Development of representative metal-free-based photocatalysts for photocatalytic overall H_2O_2 production.

by mimicking natural photosynthesis [21–23]. The sunlight-driven O_2 reduction and H_2O oxidation is considered a feasible strategy for replacing AQ oxidation process [24–28]. However, most photocatalytic H_2O_2 synthesis research and reviews primarily on the oxygen reduction reaction (ORR), while studies on the water oxidation reaction (WOR) remain limited [13,29,30]. This review focuses on photocatalytic overall H_2O_2 generation, which involves both O_2 reduction and H_2O oxidation. The choice of photocatalyst plays a crucial role in enhancing the efficiency of the photocatalytic process.

For a long time, the research on photocatalytic H_2O_2 synthesis has predominantly centered on inorganic photocatalysts, such as TiO_2, $BiVO_4$, WO_3, ZnS and CdS-based materials [4,29,31,32]. However, these materials suffer from inherent drawbacks, including a narrow absorption range, low sunlight utilization efficiency (particularly in the ultraviolet region), and limited variability, which restricts their widespread application in photocatalytic H_2O_2 generation field [9,10,14]. Various strategies-such as micro/nano structuring, surface defect engineering and heterojunctions formation-have been proposed to improve the optoelectronic properties of inorganic semiconductors. However, the efficiency of H_2O_2 production with these materials remain unsatisfactory.

Recently, metal-free organic polymers-including covalent organic frameworks (COFs), covalent triazine frameworks (CTFs), and carbon nitrile (g-C_3N_4) have attracted significant attention due to their unique optical and electrical properties [21,33–37]. These materials offer notable advantages, such as facile designability, tunable functionality, large specific surface area, and porosity, which enhance interaction between O_2/H_2O molecules and catalytic active centers, thereby improving the photocatalytic efficiency [38–41]. Moreover, the extended π-conjugation of organic polymers broadens the visible absorption range and promotes photoinduced charge separation, thereby suppressing electron-hole recombination and maximizing solar energy utilization [42–44]. In addition, the designable modular structure and versatile functionalities of organic polymers provides huge potential for the applications of photocatalysis in regulating photocatalyst composition, optoelectronic characteristics, and inter-facial properties at the atomic and molecular level [15,45,46]. So that conduction band (CB) and valence band (VB) potential of metal-free photocatalysts to simultaneously meet the requirements of redox reaction of O_2 and H_2O. These unique characteristics have received much attention and led to the rapid development of metal-free based photocatalysts with interesting structures features, but there is an urgent need to summarize and highlight the research status of metal-free photocatalytic systems for photocatalytic overall H_2O_2 generation. This review aims to summarize the process of metal-free organic photocatalysts in photocatalytic overall H_2O_2 generation and provides in-depth insight into the synthetic strategy of metal-free photocatalysts to improve photocatalysis performance (Fig. 1). First, the fundamental principles of photocatalytic overall H_2O_2 generation

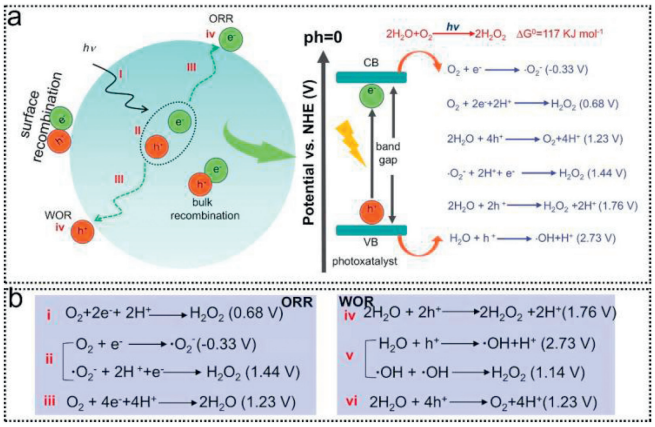


Fig. 2. Schematic of the processes involved in (a) photocatalytic overall H_2O_2 generation and (b) corresponding redox potentials.

were explicated. Then, we discuss various strategies for designing and synthesizing metal-free based photocatalysts including g-C_3N_4, CTFs, and COF to enhance their photocatalytic performance. The reaction mechanism is also analyzed to promote a deeper understanding of photocatalytic overall H_2O_2 production. Additionally, we explore the structure-activity relationships that guide the development of high-performance metal-free photocatalytic systems. Ultimately, this review aims to provide readers with a comprehensive understanding of the critical role of metal-free photocatalysts in the overall H_2O_2 generation and offer strategic insights for further improving their photocatalytic performance.

2. Fundamental principles of photocatalytic H_2O_2 production

Artificial photosynthesis on semiconductors can be divided four typically steps: light absorption inducing excitation formation, carrier separation, carrier transfer to surface of photocatalysts, and subsequent surface redox reactions (Fig. 2a) [37,47–53]. Together, these four steps determine the photocatalytic efficiency. Under illumination of light, semiconductor absorbs photons with energies greater than its band-gap, upon which generating photo-excited electrons and holes at the CB and VB, which subsequently migrate to the surface of photocatalyst for initiate the redox reaction [22,24,54,55]. To realize excellent performance, photocatalysts should keep efficient in all these four steps. In principle, photocatalysts with narrow band-gap can maximize the utilization of photons. On the other hand, to drive surface redox reactions, the minimum band-gap value should be satisfied, so that the conduction and valence band edges pass through the potential of the target redox reactions, respectively [23,26,40,56]. Therefore, when adjusting the band-gap of photocatalysts materials, the delicate balance between light absorption and band edges should be kept in mind. In addition, charge separation and transfer also play a vital role in determining the final photocatalytic performance.

As for photocatalytic overall H_2O_2 synthesis, it mainly includes ORR and WOR processes [13,30,57]. Fig. 2b showed the reaction energy barrier of ORR and WOR, *vs.* normal hydrogen electrode (NHE). The ORR reaction process contains two ways, which is direct one-step $2e^-$ ORR (i) and indirect two-step $1e^-$ ORR (ii), respectively. And the one-step $2e^-$ ORR process exhibits a more favorable energy level than indirect two-step $1e^-$ ORR. The generated $\cdot O_2^-$ from two-step $1e^-$ ORR not only has a more negative energy level (−0.33 V) than one-step $2e^-$ process but also is rather to involve in other redox reactions [4,9,10,13]. Therefore, the efficiency and selectivity of the two-step $1e^-$ pathway for producing H_2O_2 are much lower than one-step $2e^-$ ORR. Optimization the composi-

tion and structure of semiconductor photocatalysts to enhance the efficiency and selectivity of the one-step 2e⁻ ORR pathway is an effective guidance for photosynthesis H_2O_2. Similarly to the ORR process, the direct WOR also include several different reaction pathways, such as direct one-step 2e⁻ WOR, indirect one-step 2e⁻ WOR and 4e⁻ WOR processes [14]. Likewise, the direct WOR is thermodynamically more advantageous, while the indirect WOR is kinetically more favorable [21,37]. The direct one-step 2e⁻ WOR is carried out by oxidation photo-generated holes (iv), with an oxidation potential of up to 1.76 V. Indirect two-step 1e⁻ WOR can be used for photosynthesis of H_2O_2 (v), but the production of H_2O_2 from the coupled ·OH induced by hole requires a high concentration of ·OH, which is almost not limited to increasing the yield of photosynthesis H_2O_2 [31,48]. Besides, the competitive reaction of converting H_2O to O_2 and H^+ by a one-step 4e⁻ process (1.23 V, vi) inevitably happens simultaneously, resulting in a reduced H_2O_2 formation efficiency and selectivity for semiconductor photocatalysts [31,49,50]. To achieve efficient photosynthesis H_2O_2 without sacrificing reagents, it is necessary to simultaneously carry out O_2 reduction and H_2O oxidation reactions. Obviously, ORR process is theoretically easier to achieve than WOR process for photocatalytic synthesis of H_2O_2. Therefore, how to realize high-efficient WOR process is the key to achieve photocatalytic overall H_2O_2 synthesis [30,58–60].

The generation intermediates during ORR and WOR process can be measured by different *in situ* experimental characterizations, including *in-situ* Raman and diffuse reflectance infrared Fourier transform spectroscopy (DRIFTS) due to *in situ* characterization technology allows us to real-time observation the redox reaction process. Thus, *in situ* characterization is gradually developing to an advanced research strategy in materials, catalysis, and energy [4,34]. Additionally, the reaction barrier of ORR and WOR can be calculated by theoretical calculations. Currently, the theoretical calculations is a powerful method to clarify the reaction process in detail [2,11].

Based on the above result, metal-free photocatalysts have shown significant potential in the field of photocatalytic overall H_2O_2 production and have become an indispensable component in this field. Although some research on metal-free organic polymer for H_2O_2 generation has been reported, there is still a lack of related reviews to summarize the photocatalytic overall H_2O_2 generation of metal-free organic polymer for. Based on this, we will introduce the research process of representative metal-free organic polymer photocatalysts mainly including COFs, CTFs and g-C_3N_4 in overall H_2O_2 generation in recent years in the next section.

3. Photocatalytic overall H_2O_2 production by metal-free photocatalysts

3.1. The design and synthesis of metal-free-based photocatalysts

Compared with traditional inorganic photocatalysts, organic polymers possess the simple synthesis methods, strong designability, and excellent response to visible light, therefore, it holds great promise in photocatalytic overall H_2O_2 production [61–67]. Based on the abundant synthesis methods of organic polymers, their photoelectrochemical properties can be highly modulate by adjusting their structure at molecular level [68–71]. Currently, the chemical design synthesis of organic photocatalysts is mainly divided into intrinsic molecular structure and heterostructure design [44,72–75]. The intrinsic molecular structure design mainly relies on deliberately selecting suitable building blocks and linkages for modulating photoelectric properties of the polymers, thereby improving photocatalytic efficiency. Metal-free-based photocatalysts can be designed to harvest wide range light when showing exceptional stability under various operational conditions. Single-component photocatalysts usually face a fundamental contradiction: a narrow bandgap enables wide solar absorption but exacerbates rapid electron-hole recombination due to strong coulomb interactions [76,77]. Therefore, it is necessary to design the photocatalyst to decrease the recombination rate of photo-excited carriers and widen the range of light absorption. Two types of semiconductors with different staggered band structures to form heterojunctions can not only broaden the absorption range of light, but also adjust the band-gap structure. To promote the separation and transfer of carriers, the construction of heterojunction is an effective way to solve the sunlight absorption and the electron-hole pairs recombination [71,78]. Of course, there are many other efficient strategies for photocatalytic overall H_2O_2 production, such as microenvironment regulation, spin state regulation as well as amorphous 2D layered materials. These strategies could effective regulation the electronic band structures, microtopograph and physicochemical properties of photocatalysts.

Table 1
Summary of the reported g-C_3N_4 based photocatalysts for photocatalytic overall H_2O_2 production.

Photocatalyst	SCC (%)	AQY (%)	Ref.
g-C_3N_4/PDI	–	–	[83]
g-CN-MI-40	–	–	[84]
Ni-CAT-CN60	0.1	0.96@420 nm	[85]
ORP/GCN	–	–	[86]
AQ/U-POCN	–	–	[87]
SCN5	–	–	[88]
CN/CML	–	–	[89]
NiSAPs-PuCN	0.82	10.9@420 nm	[90]
CNIO-GaSA	0.4	9.1@459 nm	[91]
homo-CN	0.19	25.7@420 nm	[92]
CoOx-NvCN	0.47	5.73@420 nm	[93]
40 %K^+/I^--CN/CdSe-D	–	–	[94]
TA-CN-3	0.34	1.7@420 nm	[95]
MOC-AuNP/g-C_3N_4	–	–	[96]
CN-DMAP-GLU	–	0.792@420 nm	[97]
pH-MCN	–	–	[98]
HCP-24	–	2.38@420 nm	[99]

3.2. Photocatalytic overall H_2O_2 production by g-C_3N_4

g-C_3N_4 have shown promising in photocatalysis overall H_2O_2 filed due to its unique characteristics, such as band structure, easily manufactured, excellent chemical and thermal stability, and environmental friendliness [56,79–81]. The highly delocalized π-conjugated system is formed by sp^2 hybridization of C and N resulting in a typical semiconductor property of g-C_3N_4. It can be synthesized by simple sintering of nitrogen-rich precursors, such as melamine, cyan-amide, thiourea, and urea. The optical band gap of g-C_3N_4 at 2.7 V, with CB −1.3 V, which is more negative than the potential of O_2 reduction to H_2O_2. And the VB is located at +1.4 V, which meets the potential energy requirement of 4e⁻ H_2O oxidation. Thus, recent research has highlighted the potential of g-C_3N_4 in photocatalytic overall H_2O_2 generation from pure water and O_2 under visible light irradiation [60,80,82]. Table 1 summarizes some typical examples of photocatalytic overall H_2O_2 generation of recent g-C_3N_4-based photocatalysts [83–99]. In 2014, Hirai's group first reported photocatalytic overall H_2O_2 production using g-C_3N_4 (Fig. 3a) [83]. They found incorporating pyromellitic diimide (PDI) into g-C_3N_4 could positively shift the oxidation and reduction potentials due to the strong electron affinity of PDI. As shown in Fig. 3b, the CB and VB of g-C_3N_4/PDIx all become more positive after incorporate PDI, thus resulting in the enhanced photocatalytic water oxidation performance. Notably, g-C_3N_4/PDIx not only showed a decreased narrowed band gap for extended light response range but also had a deeper VB position than g-C_3N_4 which

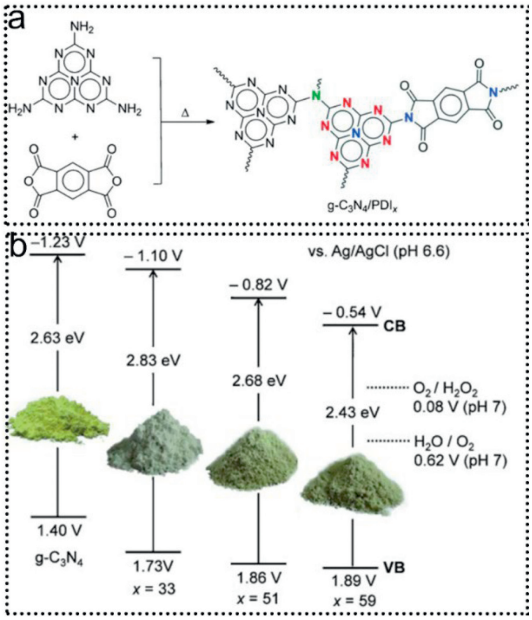


Fig. 3. (a) Synthesis process for g-C_3N_4/PDIx. (b) Electronic band structures of g-C_3N_4 and g-C_3N_4/PDIx. Copied with permission [83]. Copyright 2014, Wiley-VCH Verlag GmbH & Co. KGaA, Weinheim.

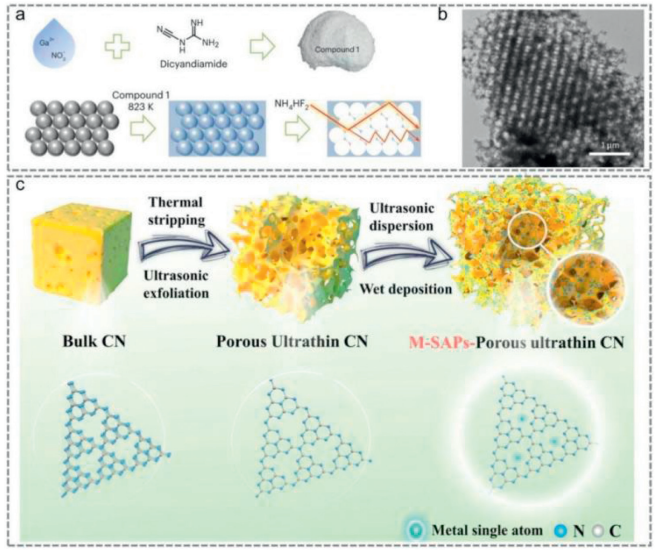


Fig. 4. (a) Synthetic process of CNIO-GaSA. (b) SEM image of CNIO-GaSA. Copied with permission [91]. Copyright 2022, Springer Nature. (c) Schematic diagram of the synthesis of high-loading MSAPs-PuCN. Copied with permission [90]. Copyright 2023, Springer Nature.

possessed enough thermodynamic driving force to enhance photocatalytic water oxidation ability. The apparent quantum yield (AQY) test was consistent with the energy band structure of g-C_3N_4/PDIx, indicating that the optimized band-gap structure could promote water oxidation and O_2 reduction. After that, various methods for preparing highly active g-C_3N_4 for photocatalytic overall H_2O_2 evolution have been developed, including construction of single-atom doped, heterostructures and functionalization. In this part, the research process on photocatalytic overall H_2O_2 generation over g-C_3N_4-based photocatalysts are systemically summarized. And we introduce the different strategies in details to review photocatalytic overall H_2O_2 production over g-C_3N_4.

3.2.1. Single-atom doping

Single-atom has high active centers, such that unique properties exist for the ideal design of new photocatalysts with high activities, low-cost and stability [100,101]. Therefore, given the photocatalytic overall H_2O_2 generation, some optimal design of single-atom doped have been prepared and display exceptional performance in overall H_2O_2 production. Guo's group designed Ga-doped g-C_3N_4 (CNIO-GaSA) with Ga-N_4 sites, where Ga^{3+} acts as a Lewis acid to polarize adsorbed O_2, facilitating $2e^-$ reduction to *OOH. Density functional theory (DFT) calculations revealed that the Ga-doped site lowers the *OOH formation barrier by 0.3 eV compared to pristine g-C_3N_4 [91].

In situ DRIFTS spectra confirmed the presence of *OOH intermediates, validating the dominant $2e^-$ ORR pathway. However, the sluggish water oxidation kinetics ($4e^-$ WOR) limits the overall efficiency, suggesting the need for cocatalysts to improve O_2 evolution. The synthetic process of CNIO-GaSA was shown in Fig. 4a. It was prepared by combining $Ga(NO_3)_3$ and dicyandiamide as the precursor and silica opal as template with subsequent removal strategies. Partial density of states (PDOS) reveals the formation hybridized Ga 4p and N 2p states could enhance the conductivity of CN contribute to reduce the transfer resistance of charge carriers. The transmission electron microscopy (TEM) (Fig. 4b) image show that obtained CNIO-GaSA has the periodic pore structure with an average diameter of ~250 nm. CNIO-GaSA presents a significantly enhanced H_2O_2 production rate (368.5 μmol/h), which is about 4.0 and 7.8 times, respectively higher than that of CNIO and CN. In addition, CNIO-GaSA exhibits the highest catalytic activity compare to other previously reported photocatalysts. Significantly, CNIO-GaSA also shows the excellent 100 % efficiency for kill bacteria, thereby offering promising potential practical application. Although the CNIO-GaSA shows excellent photocatalytic activity toward overall H_2O_2 generation, the Ga is rare metals, which is not fit for practical application. On this basis, Zhang's group reported a high-loading Ni single-atom photocatalyst for efficient overall H_2O_2 synthesis with an AQY and solar-to-chemical conversion (SCC) up to 10.9 % and 0.82 %, respectively (Fig. 4c) [90].

They found that Ni-N_3 sites transform into high-valent O_1_Ni-N_2 sites using different *in-situ* characterizations. And the PDOS of Ni confirm that Ni 3d orbitals contribute to both CB and VB, suggesting Ni single atoms exceedingly optimize the electronic structure. Extensive experiments and detailed calculations prove that the development of the sites structure decreases the energy barrier of *OOH and inhibits the O=O bond dissociation resulting in improved H_2O_2 production activity. As shown in the proposed synthesis process, the high-loading M-SAPs can be divided into modulating the microtopography and optimizing the loading process. PuCN showed a higher overall H_2O_2 generation rate (41.1 μmol L^{-1} h^{-1}) than of BCN (16.5 μmol L^{-1} h^{-1}) due to the porous ultra-thin structure improved the contact range of O_2. Apparently, the NiSAPs-PuCN showed highest H_2O_2 generation rate up to 342.2 μmol L^{-1} h^{-1}, which was about 20.7 and 8.3 times higher than that of BCN and PuCN, respectively. Furthermore, the H_2O_2 generation activity of NiSAPs-PuCN can be improved to 640.1 μmol L^{-1} h^{-1} under AM 1.5 G irradiation. The AQY was tested owing to the AQY value is generally recognized as one of more reliable factors for assessing the photocatalytic property. Experiment demonstrated that the introduction of Ni active sites can greatly facilitate the O_2 adsorption compared to pure BCN (decreased from 1.1 eV to −0.83 eV). It is essential that format the core intermediate *OOH for overall H_2O_2 generation *via* $2e^-$ ORR. The calculation result suggest that improvement O_2 adsorption capacity can promote intermediate formation, thus improving the conversion efficiency of H_2O_2. Charge density difference calculation result showed the charge redistribution of NiSAPs-PuCN is more remarkable than BCN, suggesting the Ni sites can promote the *OOH formation. Liu's group

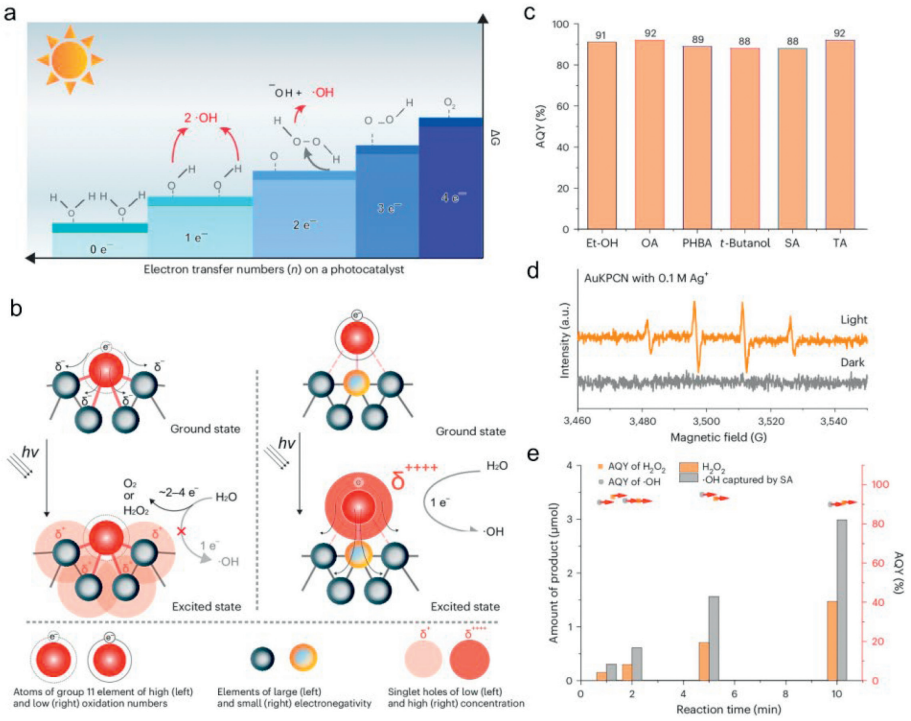


Fig. 5. (a) Schematic diagram showing the intermediates in the multielectron-transfer processes of WOR. (b) Excited properties of group 11 elements at different chemical states. (c) Average AQY of AuKPCN for photocatalytic H_2O_2 with different sacrificial agent. (d) ESR spectra of AuKPCN recorded in 0.1 mol/L $AgNO_3$ solution. (e) Generation amount of ·OH and H_2O_2 in SA with saturated O_2. Copied with permission [102]. Copyright 2024, Springer Nature.

reported atomically dispersed Au on potassium-incorporated g-C_3N_4 (AuKPCN) that could simultaneously improve photocatalytic production of ·OH and H_2O_2 (Fig. 5) [102]. Details experiments and theoretical calculations proved that the low-valent Au changed the materials' band gap structure to trap localized holes produced under photo-excitation. Fig. 5a showed the $1e^-$ WOR has the highest efficiency for ·OH production owing to one h^+ can produce one ·OH. The *in-situ* Raman and DRIFTS testing result confirm that one-electron WOR could produce ·OH and unleash proton to accelerate ORR. The Au element has s orbital and d^{10} orbitals of Au element was filled by one electron and fully electron resulting in formation a highly concentrated hole under excited state (Fig. 5b). And the AuKPCN exhibited a remarkable AQY of around 85 % at the wavelength range of 400–420 nm in different organic electron donor system (Fig. 5c). To further study the oxidation half reaction of AuKPCN, Ag^+ and DMPO were added. The electron spin resonance (ESR) test result suggests the ·OH can be detected in the presence of AuKPCN without found O_2 and H_2O_2, indicating the WOR process can produce the ·OH over AuKPCN (Fig. 5d). Significantly, the generation amount of ·OH and H_2O_2 is close to 2:1 (Fig. 5e), which consistent with the theoretical proportion based on $1e^-$ WOR. As we have seen yet, AuKPCN showed the highest AQY, which was larger than previously reported photocatalysts for produce ·OH *via* $1e^-$ and $2e^-$ WOR. This outstanding work first reports on $1e^-$ WOR generation ·OH and released the proton for enhancing the H_2O_2 production rate. But the ·OH can dissociation H_2O_2 owing to the its strong oxidizing properties.

3.2.2. Heterojunction

As well known, the single-component photocatalyst often cannot satisfy all the requirements for photocatalytic overall H_2O_2 production due to the fast photo-generated charge recombination and insatiable redox capacity [103–107]. Therefore, to decrease the recombination rate of photo-excited carriers and raise redox capacity, it is necessary to reform the photocatalyst. The construction of heterojunction by combining two kinds of semiconductors with interleaving band structure can not only decrease the recombination rate of photo-excited electron and hole, but also adjust redox capacity for fulfillment different photocatalysis requirements. Fan's group reported a binary semiconductors photocatalytic system for photocatalytic overall H_2O_2 generation [94]. Extensive experiments and calculation revealed that heterojunction can enhance light absorption capabilities and reduce interlayer charge transfer distance. They used X-ray absorption fine structure and *in situ* XPS to study coordination environment and charge transfer mechanism of heterojunction. Fig. 6a illustrated the synthesis route for K^+/I^--CN/CdSe-D heterojunction. The I^- and K^+ ion intercalation into g-C_3N_4 was achieved by the assistance of KCl/KI salt. And the composite was formed by the *in situ* modified CdSe onto K^+/I^--CN nanosheets using a microwave hydrothermal method. The photocatalytic overall H_2O_2 production activity of obtained samples was assessed under visible light irradiation. The photocatalytic performance of heterojunction surpassed that of the individual CdSe-D and K^+/I^--CN. The 40 % K^+/I^--CN/CdSe-D exhibited the highest photocatalytic activity (448.63 μmol/L), which exceeded that most metal-free photocatalysts. They also tested the photocatalytic overall H_2O_2 generation with different mass loading. The results showed a significant linear relationship between catalyst amount and the yields of H_2O_2, further suggesting the reliability of the photocatalytic activity. Further the continuous irradiation experiment demonstrated excellent photocatalytic stability of heterojunction. Remarkably, the K^+/I^--CN/CdSe-D not only exhibited the excellent photocatalytic stability, but also showed higher overall H_2O_2 generation rate than the other photocatalysts, which make it very promising photocatalyst considering its easy preparation. This study emphasizes the significance of interface chemical and ionic intercalation for enhancing the photocatalytic overall H_2O_2 generation. Tao *et al.* prepared g-C_3N_4 homojunction with functional surface for efficient photocatalytic overall H_2O_2 generation [92]. Kelvin probe force microscopy (KPFM) and calculations results

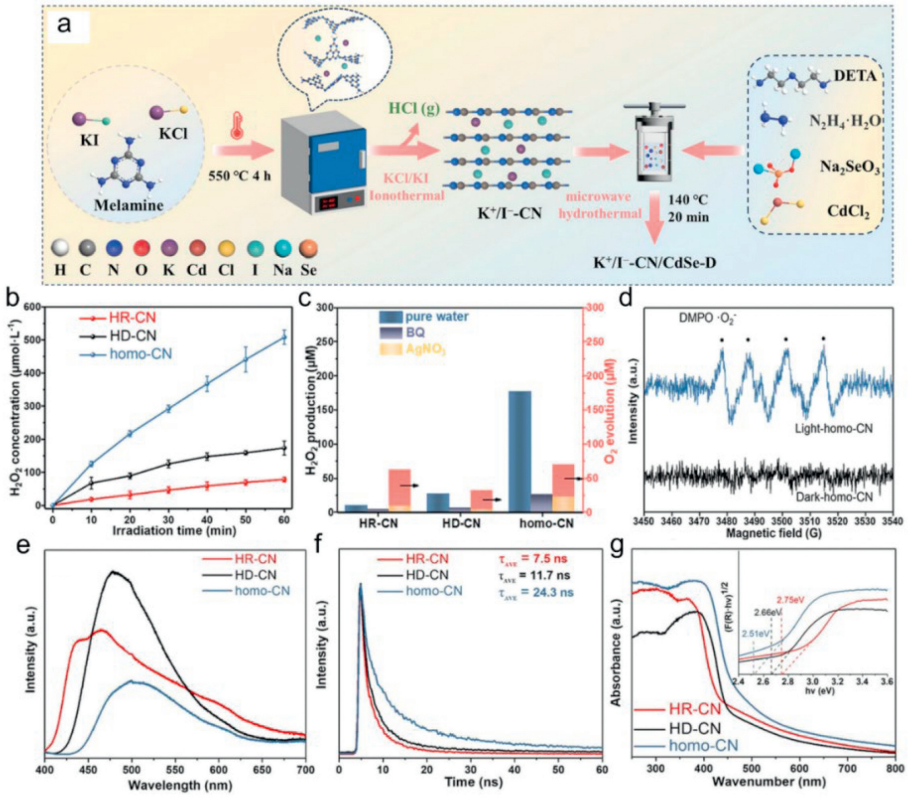


Fig. 6. (a) Schematic diagram of the synthesis K^+/I^--CN/CdSe-D. Copied with permission [94]. Copyright 2024, Wiley-VCH GmbH. (b) The H_2O_2 yield of HR-CN, HD-CN and homo-CN. (c) H_2O_2 yield of obtained samples under different conditions. (d) EPR signal of DMPO $^{\bullet}O_2^-$ of homo-CN. (e) Steady-state photoluminescence spectra and (f) fluorescence lifetime decay curves. (g) UV–vis DRS and energy band gap plots. Copied with permission [92]. Copyright 2023, Elsevier.

suggest that surface hydroxyls of g-C_3N_4 can extract electron from the bulk to the surface. The photocatalytic overall H_2O_2 production performance of homojunction is assessed under visible light irradiation. As shown in Fig. 6b, homo CN showed a highest H_2O_2 yield (508.4 μmol/L), which was about 2.9 and 6.6 times higher than HD-CN and HR-CN respectively. To demonstrate the H_2O_2 synthesis route, photocatalytic H_2O_2 generation was tested under different measurement conditions for 2 h. As shown in Fig. 6c, 177 μmol/L of H_2O_2 yield was produced in pure water by homo-CN, while HD-CN and HR-CN almost have no H_2O_2 yield. When benzoquinone (BQ) added in the reaction system, all the samples show that H_2O_2 yields reduce sharply. This result suggests that obtained samples synthesize H_2O_2 *via* two step single-electron route. Electron paramagnetic resonance (EPR) characterization results further confirm that the two step single-electron process (Fig. 6d). The steady state PL and fluorescence lifetime measurement result proved that homojunction can improve charge separation and transfer (Figs. 6e and f). UV-vis diffuse reflectance spectra (UV-vis DRS) characterization revealed that homojunction extends the visible light absorption range that is beneficial to photocatalytic overall H_2O_2 production (Fig. 6*g*).

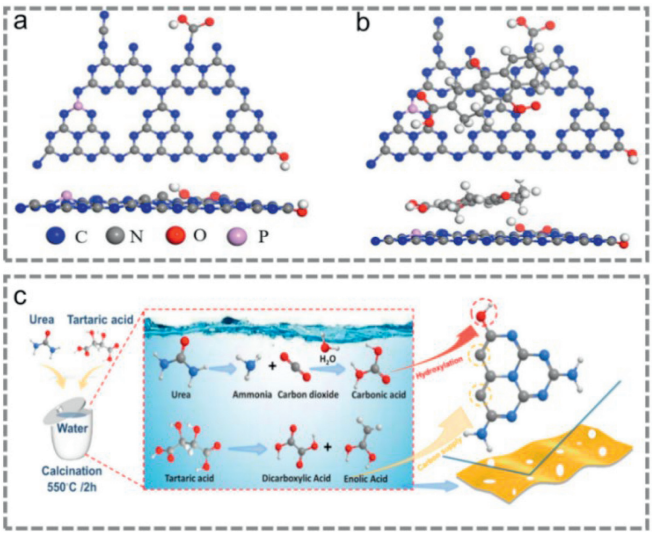


Fig. 7. Structures model of (a) U-POCN and (b) AQ/U-POCN. Copied with permission [87]. Copyright 2021, Wiley-VCH GmbH. (c) Schematic diagram of the synthesis of TA-CN sample by solution pyrolysis. Copied with permission [95]. Copyright 2024, Elsevier.

3.2.3. Functionalization

In addition to the reported heterojunction and single-atom doped strategies, functionalization and defects are also effective strategy for photocatalytic overall H_2O_2 generation. Ouyang's group reported an elaborately modified g-C_3N_4 (U-POCN and AQ/U-POCN) photocatalyst for overall H_2O_2 generation (Figs. 7a and b) [87]. The AQ/U-POCN exhibited the highest catalytic efficiency (75 μmol L^{-1} h^{-1}) ever reported without using any additives. Calculations and experiments revealed that P, O-co-doping could improve the water oxidation ability of the g-C_3N_4, which was capable of oxidation H_2O to H_2O_2 directly. Similarly, Shi's group reported tartaric acid-modified g-C_3N_4 (TA-CN) by introducing hydrophilic hydroxyl groups into the g-C_3N_4 (Fig. 7c) [95]. They found π-electron-rich can effectively reduce exciton binding energy result in increasing the transfer rate of photo-excited electrons, enabling faster migration from the production site to the active sites, thereby enhancing photocatalytic overall H_2O_2 genera-

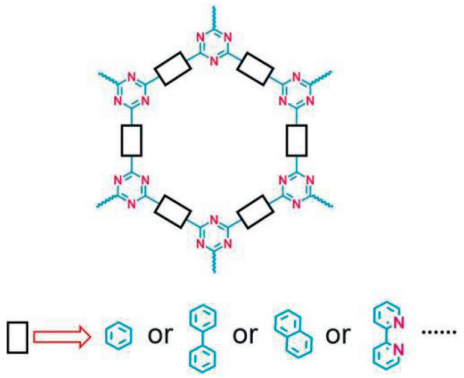


Fig. 8. The molecular structure of CTFs.

tion efficiency. Besides, the hydroxyl groups modulate reaction kinetics by enhancing the adsorption ability of intermediates by their hydrophilic intrinsic, which favors the overall reaction efficiency.

3.3. Photocatalytic overall H_2O_2 production by CTFs

CTFs are a class of organic porous materials formed by covalent bonding with a triazine ring as the structural unit, typically obtained from nitrogen-rich aromatic precursors by polymerization reaction (Fig. 8) [58]. While CTFs are a branch of the COFs family, their unique triazine ring structure endows them with exceptional physicochemical properties and remarkable stability [63,108,109]. In 2008, Kuhn *et al.* successfully obtained the first CTFs material (CTF-1) under ionothermal conditions [110]. This pioneering work not only established the foundation for the exploration and development of CTFs but also opened the door to their extensive applications across energy, catalysis and adsorption and separation.

In recent years, CTFs have gradually become a promising catalytic platform for the photocatalytic overall H_2O_2 generation by virtue of their unique photophysical properties [111,112]. Their advantages for overall H_2O_2 production can be attributed to several key factors, including (1) abundant N atoms, high specific surface area and ordered pore structure that can promote oxygen adsorption, activation, and transport; (2) structural tunability provides remarkable flexibility to enhance the selectivity and yield of H_2O_2 production; (3) unique π-conjugated structure in the triazine ring facilitates efficient long-range migration of photo-generated electrons; (4) highly stable C≡N bonds endow the catalyst with excellent durability under acidic, basic and complex reaction conditions. Nevertheless, CTFs still face some key challenges in the photocatalytic production of H_2O_2, such as the rapid recombination of photo-generated charge carriers, sluggish reaction kinetics, and the inherently high impedance and low electrical conductivity characteristic of organic semiconductors, which greatly limit the further enhancement of photocatalytic efficiency [113–115]. To address these challenges, recent research has introduced a range of innovative strategies, including the modulation of the framework structure, the introduction of heterojunction and the optimization of the electron transfer pathway, which provide new ideas and directions to achieve a breakthrough in the photocatalytic production of H_2O_2 by CTFs [116–118].

3.3.1. Introducing the functional groups

In 2019, Xu's group first reported photocatalytic overall H_2O_2 production using functionalized CTFs [30]. They found that introducing acetylene or diacetylene groups into CTFs (CTF-BPDCN, CTF-EDDBN, and CTF-BDDBN) can significantly enhance photocatalytic H_2O_2 production rate due to the reduced energy associated with OH^* formation and thus enable a new $2e^-$ oxidation route toward overall H_2O_2 generation. As shown in Fig. 9a, CTFs with acetylene and diacetylene are prepared from their corresponding nitrile precursors. They tested the photocatalytic overall H_2O_2 generation performances of different samples in pure water under visible light irradiation. The average H_2O_2 generation rate of the CTF-BDDBN was calculated to be 79 μmol, which was about 2 and 3.8 times higher than that of CTF-BPDCN and CTF-EDDBN (Fig. 9b). Moreover, the SCC efficiency of the best-performing CTF-BDDBN is measured to be 0.14% (Fig. 9c), which was larger than previously reported organic photocatalysts. Further theoretical calculations revealed alkynyl groups can develop a new $2e^-$ oxidation route toward overall H_2O_2 production (Figs. 9d and e). After that, Han *et al.* developed a thiourea-functionalized CTF (Bpt-CTF) through a polarization engineering strategy, effectively addressing the sluggish kinetics of H_2O_2 production during $2e^-$ oxygen photoreduction (Fig. 9f) [119]. Photocatalytic performance tests showed that the Bpt-CTF greatly enhanced H_2O_2 production by $2e^-$ ORR from water and O_2. The H_2O_2 production rate reached 3268.1 μmol h^{-1} g^{-1} of Bpt-CTF without the use of any sacrificial agents or co-catalysts, which was more than an order of magnitude improvement compared to Dc-CTF. Mechanistic studies revealed that the superior photocatalytic activity of Bpt-CTF was attributed to the incorporation of the (thio)urea functional group, which greatly enhanced the polarization of the CTFs, thereby significantly promoting charge separation and optimizing the electron transfer dynamics. Previously reported on functionalized CTFs are widely limited by the amorphous or weakly crystalline structure. Generally, improved the crystallinity of organic materials can accelerate charge transport and separation in the skeleton, which is conducive to their photocatalytic application. In view of this, Xu's group successfully synthesized two high-crystalline CTFs with 1,1′-biphenyl-4,4′-dicarbonitrile (BP-CN) and 9*H*-fluorene-2,7-dicarbonitrile (FL-CN) as the building blocks (Figs. 10a and b) [37]. Notably, the exfoliated CTF-FL exhibited an exceptional H_2O_2 production rate of 5007 μmol g^{-1} h^{-1} from O_2 and pure water under sacrificial agent-free conditions, significantly surpassing all previously reported CTF-based photocatalysts and establishing itself among the most efficient metal-free H_2O_2 photocatalytic systems to date. And femtosecond-transient absorption (fs-TA) spectroscopy characterization results confirm the locked-in molecular architecture suppress rapid recombination of photoexcited carriers. Time-resolved photoluminescence (TRPL) analysis demonstrated spatially locked structure could extended π-electron delocalization and enhance strong intermolecular interaction (Fig. 10d). Structural characterization and theoretical calculations further reveal that the outstanding photocatalytic performance of CTF-FL stems from its spatially locked structure, which not only enhances the efficiency of separation and transfer of photo-excited charge-carriers, but also regulates the local electronic structure, leading to a shift of the WOR pathway to shift from the $4e^-$ to the $2e^-$ process, and ultimately achieves 100% atom utilization efficiency. And the overall H_2O_2 generation test was performed under AM 1.5 G one-sun illumination. Remarkably, the SCC efficiency of exfoliated CTF-FL reached up to 0.91%, which exceed the most metal-free photocatalysts ever reported (Fig. 10c). Total density of states (TDOS) results suggest agreement with the experimental results of band gaps for CTF-FL (2.41 eV) and CTF-BP (2.52 eV). The reaction barrier is calculated to further understand the photocatalytic overall H_2O_2 production mechanism. The calculation result suggests that the spatially locked can reduce the barrier of ORR and WOR resulting in boosting efficient overall H_2O_2 production (Figs. 10e and f).

3.3.2. Functionalization

Inspired by the stepwise energy- and charge transfer processes in natural photosynthesis, Zhang and co-worker designed

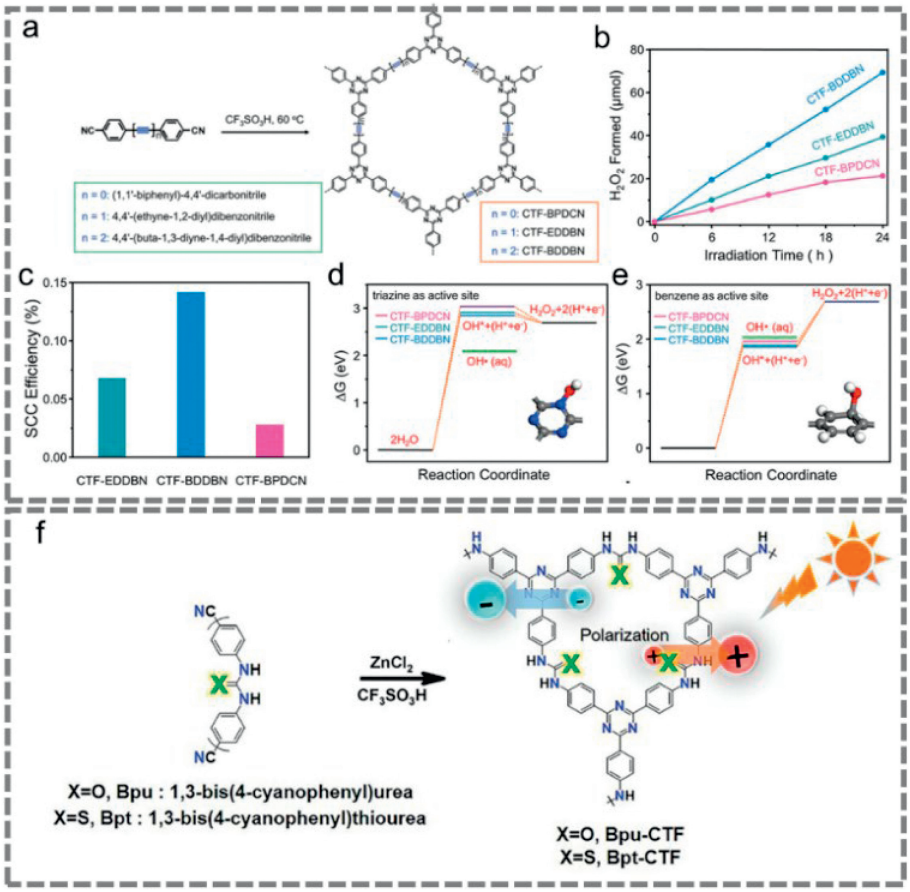


Fig. 9. (a) Scheme of the synthesis of samples from their precursors. (b) Typical time course of H_2O_2 production using different samples. (c) The SCC efficiencies measured under simulated AM1.5 G. Calculated free energy different active sites: (d) Triazine structure in all CTFs, (e) benzene group in all CTFs. Copied with permission [30]. Copyright 2019, Wiley-VCH GmbH. (f) Rational synthesis of samples with different charge separation and transfer ability. Copied with permission [119]. Copyright 2022, Wiley-VCH GmbH.

and synthesized three CTFs with stepwise charge transfer functionality (asy-CTF, Ace-asy-CTF and Th-asy-CTF) (Figs. 11a and b) [120]. Without the presence of a sacrificial agent, the Ace-asy-CTF showed the highest photocatalytic overall H_2O_2 generation performance compare to asy-CTF and Th-asy-CTF. The AQY of Ace-asy-CTF was determined under different monochromatic wavelengths. The AQY of Ace-asy-CTF reached 4.4 % at 420 nm wavelength. Furthermore, Ace-asy-CTF showed a SCC efficiency up to 0.48 % under AM 1.5 G simulated sunlight illumination. The long-term recycling tests suggests that Ace-asy-CTF possessed excellent photocatalysis stability. *In situ* characterization and theoretical calculations revealed that the acetylene units in Ace-asy-CTF as key site for efficient charge separation and exciton transport through a stepwise charge transfer mechanism, thus enhancing the photocatalytic activity of the Ace-asy-CTF. The inherent high impedance and suboptimal electrical conductivity of CTFs still limit their charge transfer ability during photocatalysis. For this reason, Zhou *et al.* successfully prepared bonded CQD-CTF photocatalysts by embedding carbon quantum dots (CQDs) into the pores of CTFs (Fig. 11c) [55]. The optimized 0.5 % CQD-CTF exhibited excellent H_2O_2 production activity in a pure water system without sacrificial agent, achieving a generation rate as high as 1036 μmol g^{-1} h^{-1}, which was 4.6 times higher than that of the original CTF. Theoretical calculations and *in situ* characterization further elucidated the incorporation of CQDs not only improved the electrical conductivity of CTFs but also strengthened their proton affinity and oxidative capability, thereby markedly boosting the catalytic performance of 0.5 % CQD-CTF in both the ORR and WOR.

3.3.3. Single-atom doped

In addition to the reported heterojunction and functionalization strategies, single-atom doped in CTFs for photocatalytic overall H_2O_2 production has also been extensive studied. Shen's group prepared a high-density Co single-atom-loaded pyridine modified CTF (CoSA/Py-CTF) for photocatalytic overall H_2O_2 generation (Fig. 12a) [121]. The obtained CoSA/Py-CTF exhibited a remarkable photocatalytic overall H_2O_2 evolution rate of 2898.3 μmol g^{-1} h^{-1} under visible light irradiation with an AQY and SCC up to 13.2 % at 420 nm and 0.15 % under AM 1.5, respectively, which exceed most metal-free photocatalysts ever reported. The FT-IR and XRD demonstrated the single-atom-loaded CTF was prepared successfully (Figs. 12b and c). This research provides perceptive observations into the intricate dynamic behavior and catalytic mechanism of SACs. After that, Shen's group further study photocatalytic overall H_2O_2 evolution using Ni single-atom doped CTFs (Fig. 12d) [122]. They found dual-pathway synergistically promoting photocatalytic overall H_2O_2 evolution by ORR and WOR. Dual active site CTFs loading single-atom Ni and pyridine N (d-CTF-Ni) presented excellent overall H_2O_2 evolution rate of 869.1 μmol g^{-1} h^{-1}. This study offers a new insightful on the dual active site catalytic mechanism for photocatalytic overall H_2O_2 generation.

3.4. Photocatalytic overall H_2O_2 production by COFs

COFs are a classic representative of porous organic polymers with high crystallinity and periodic structures. The COFs usually are synthesized using reversible chemical reactions, such as borox-

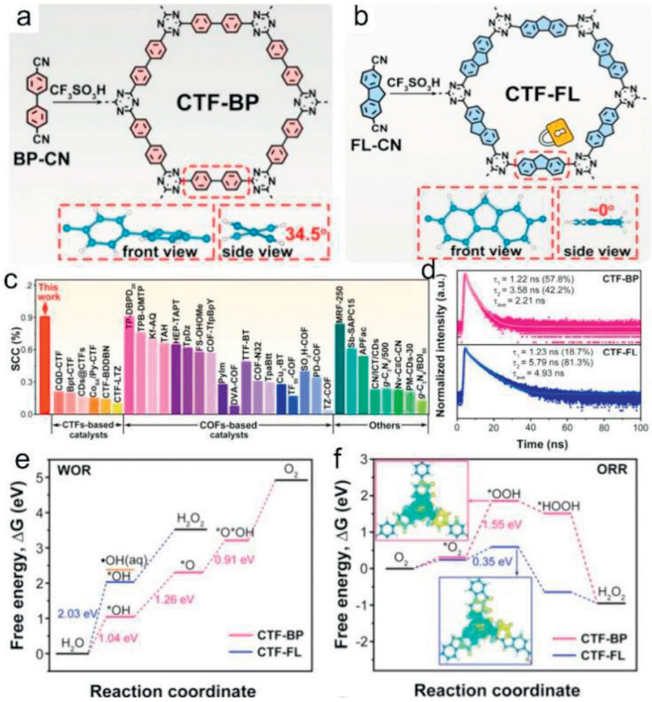


Fig. 10. Schematic diagram for synthesizing of (a) CTF-BP and (b) CTF-FL. (c) Comparison of the SCC efficiency for CTF-NSs with the reported representative metal-free photocatalysts; (d) Time-resolved PL spectra of CTF-BP (pink) and CTF-FL (blue); Gibbs free energy diagrams of (e) ORR and (f) WOR steps on CTF-BP and CTF-FL. Copied with permission [37]. Copyright 2024, American Chemical Society.

ine, boronate-ester, imide, and imidazole, thus, leading to highly crystallinity [123–125]. In 2005, Yaghi's research group first successfully prepared COF-1 and COF-5 by reversible boronate-ester reaction (Fig. 13) [123]. Over the past few years, the COFs materials with different linkages develop rapidly due to their exactly structural characteristics and great potential in various field, such as en-

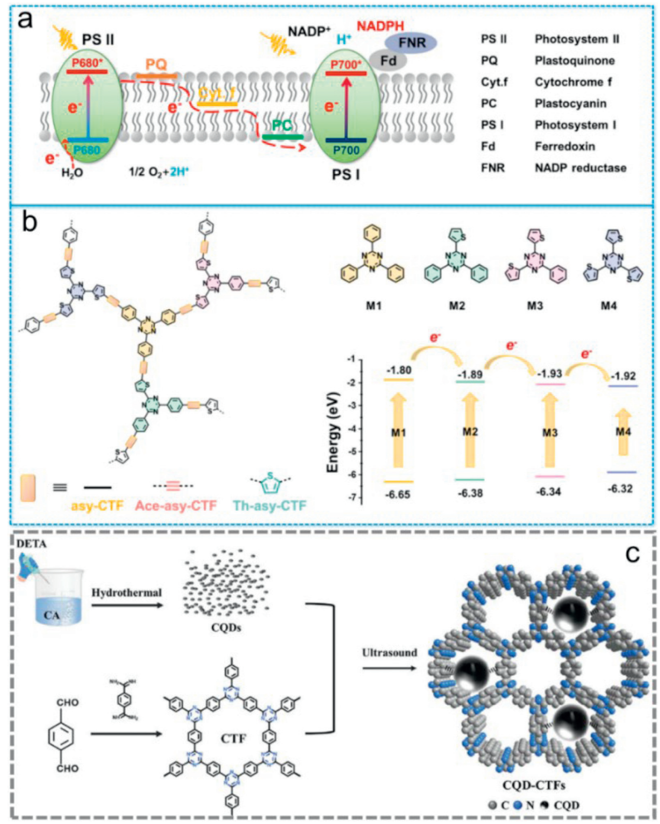


Fig. 11. (a) Natural photosynthesis charge separation processes. (b) Schematic illustration of the stepwise charge transfer within the CTFs. Copied with permission [120]. Copyright 2024, American Chemical Society. (c) Scheme of the synthetic route of CQD-CTFs. Copied with permission [55]. Copyright 2024, Wiley-VCH GmbH.

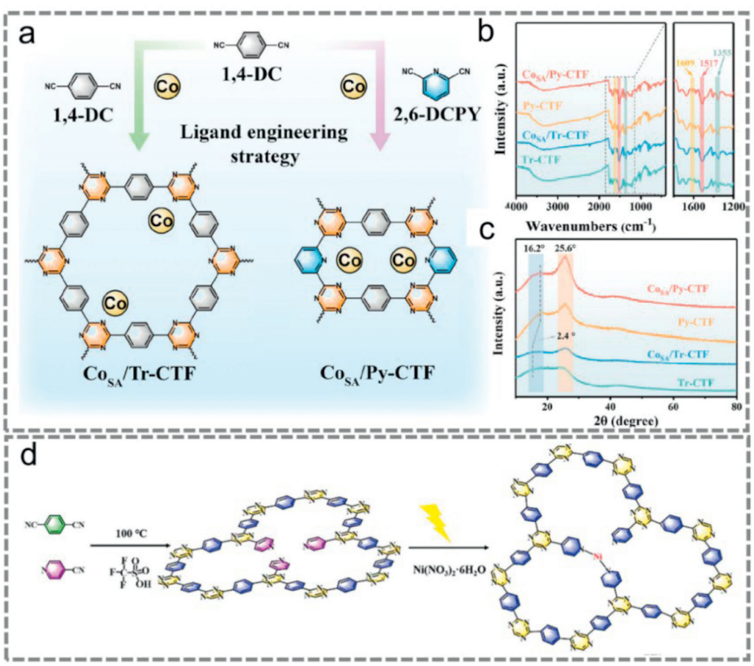


Fig. 12. (a) Synthetic routes of CoSA/Tr-CTF and CoSA/Py-CTF. (b) FT-IR spectra and (c) XRD pattern of samples. Cpied with permission [121]. Copyright 2024, American Chemical Society. (d) The synthesis strategy and structure of d-CTF-Ni. Copied with permission [122]. Copyright 2024, Elsevier.

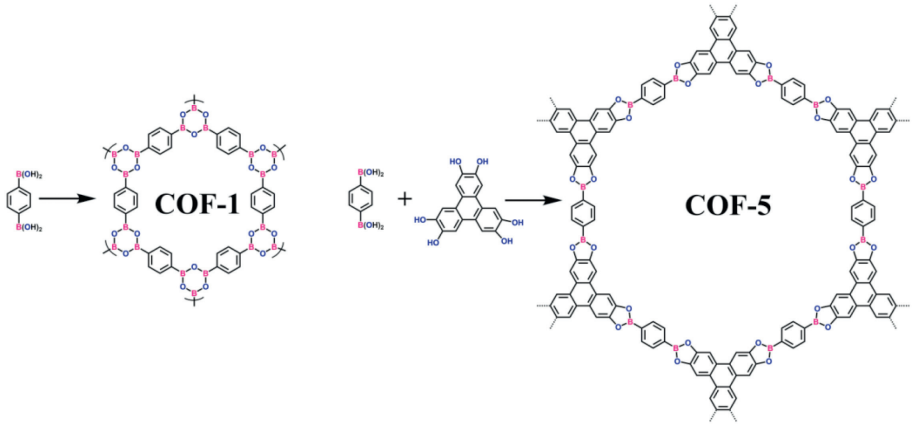


Fig. 13. Structure model of COF-1 and COF-5.

ergy storage and conversion, separation and photo/electron catalysis (Fig. 14) [126–132]. The COFs with semiconductor characteristics are one of the promising candidate materials for overall H_2O_2 production due to their large surface area, structural designability, high chemical stability, light weight, extensive π-conjugation, flexible synthetic strategy. The extensive π-conjugation in COFs extended covalent systems promotes the absorbance of visible light. The π-π stacking interaction of framework benefit the migration and transport of carriers, which can prevent the recombination of photo-excited carriers and maximize photocatalytic overall H_2O_2 production efficiency. The larger surface area can expose abundant active sites and promote contact between water and COFs frameworks. It is the synthesis link-ages modules provide rich options for design production with different photo-electric and physical properties for various application. Given these unique properties, COFs have shown satisfactory employment in photocatalytic overall important that H_2O_2 production, and many of them have exhibited better performance than inorganic semiconductors [133]. However, the COF's photocatalytic overall H_2O_2 production was not achieved until 2021, which is far behind other photocatalytic applications such as water splitting, CO_2 reduction, and organic degradationc [134–136]. In 2021, Yu's group first reported photocatalytic overall H_2O_2 production using triphenylbenzene-dimethoxyterephthaldehyde-COF (TPB-DMTP-COF) at gas–liquid–solid interface (Fig. 15a) [134].

The reported TPB-DMTP-COF can efficient reduce O_2 to H_2O_2 in a wide pH range and pure water condition (Fig. 15b). TPB-DMTP-COF showed a high H_2O_2 generation rate of 2882 μmol g^{-1} h^{-1} under visible light irradiation due to the high crystallinity and large specific surface area as high as 2747 m^2/g (Fig. 15c). More importantly, a solar-to-chemical conversion of 0.76% is achieved for H_2O_2 generation surpassing most of the metal-free photocatalysts ever reported. This study provides fundamental insights into the reasonable designed synthesis of highly efficient metal-free photocatalysts for overall H_2O_2 generation by precise control over photocatalytic reaction pathways. Since then, the continuous efforts have been devoted to design COFs resulting in rapid development of COFs-based photocatalytic systems with various structure and properties preference through different strategies. In this section, the research advance on photocatalytic overall H_2O_2 generation over COFs and COF-based heterojunction for enhancing photocatalytic performance are systematic summarized and discussed in detail. Some typical examples of photocatalytic overall H_2O_2 generation by COFs are summarized in below Table 2 [13,18,19,43,57,134,137–147]. And we present the differently strategies, such as functional group modification, introducing donor-acceptor, and COFs nanohybrids, to review photocatalytic overall H_2O_2 production over COFs and its heterojunction.

Table 2
Some examples of photocatalytic H_2O_2 generation by COFs.

Photocatalyst	SCC (%)	AQY (%)	Ref.
TPB-DMTP	0.76	18.4@420 nm	[134]
TF50-COF	0.17	5.1@400 nm	[18]
COF-TfBpy	1.08	13.6@420 nm	[19]
TTF-BT-COF	0.49	11.9@420 nm	[137]
TD-COF	0.15	–	[138]
HEP-TAPT	0.65	15.35@420 nm	[139]
COF-N_{32}	0.31	6.2@459 nm	[43]
TpDz	0.62	11.9@420 nm	[140]
Py-Da-COF	0.09	4.5@420 nm	[141]
TaptBtt	0.296	–	[142]
TZ-COF	0.036	0.6@475 nm	[143]
Kf-AQ	0.7	15.8@400 nm	[131]
TB-COF	1.08	–	[144]
TPB-COF-OH	0.84	9.61@420 nm	[57]
DVA-COF	0.08	2.84@420 nm	[130]
COF-2CN	0.6	6.8@459 nm	[129]
TBD-COF	1.04	–	[145]
QH–HPTP-COF	1.41	–	[13]
TAH–COF	0.66	7.72@420 nm	[146]
DHAA	0.23	4.6@380 nm	[147]

3.4.1. Introducing functional groups

Introducing functional groups into organic semiconductors is well known as an effective strategy to endow semiconductors with unique characteristic [54,135,136,148–150]. Firstly, the well design functional groups can modulate the photo-electronic properties of COFs, enhance visible light response and improve the photo-excited carriers separation efficiency [148]. Additionally, the modified special groups can change the stability of COFs under different environment, holding the catalytic stability over long time testing. Importantly, incorporation the functional groups can optimize the efficiency of charges transfer, decrease the recombination of electron-hole pairs and improve the yield of H_2O_2 [75]. Hou and co-authors reported a simple and efficient strategy for the synthesis a class of COFs photocatalysts with multiple charge transfer channels by introducing dicyano-functional group (Figs. 16a-c) [151]. As a result, COF-2CN with multiple charge transfer channels exhibits the significantly higher H_2O_2 generation rate (1601 μmol g^{-1} h^{-1}) than other samples (Fig. 16d). This suggests that dicyano-functional group in COFs can greatly improve the overall generation efficiency of H_2O_2. Moreover, the AQY and SCC

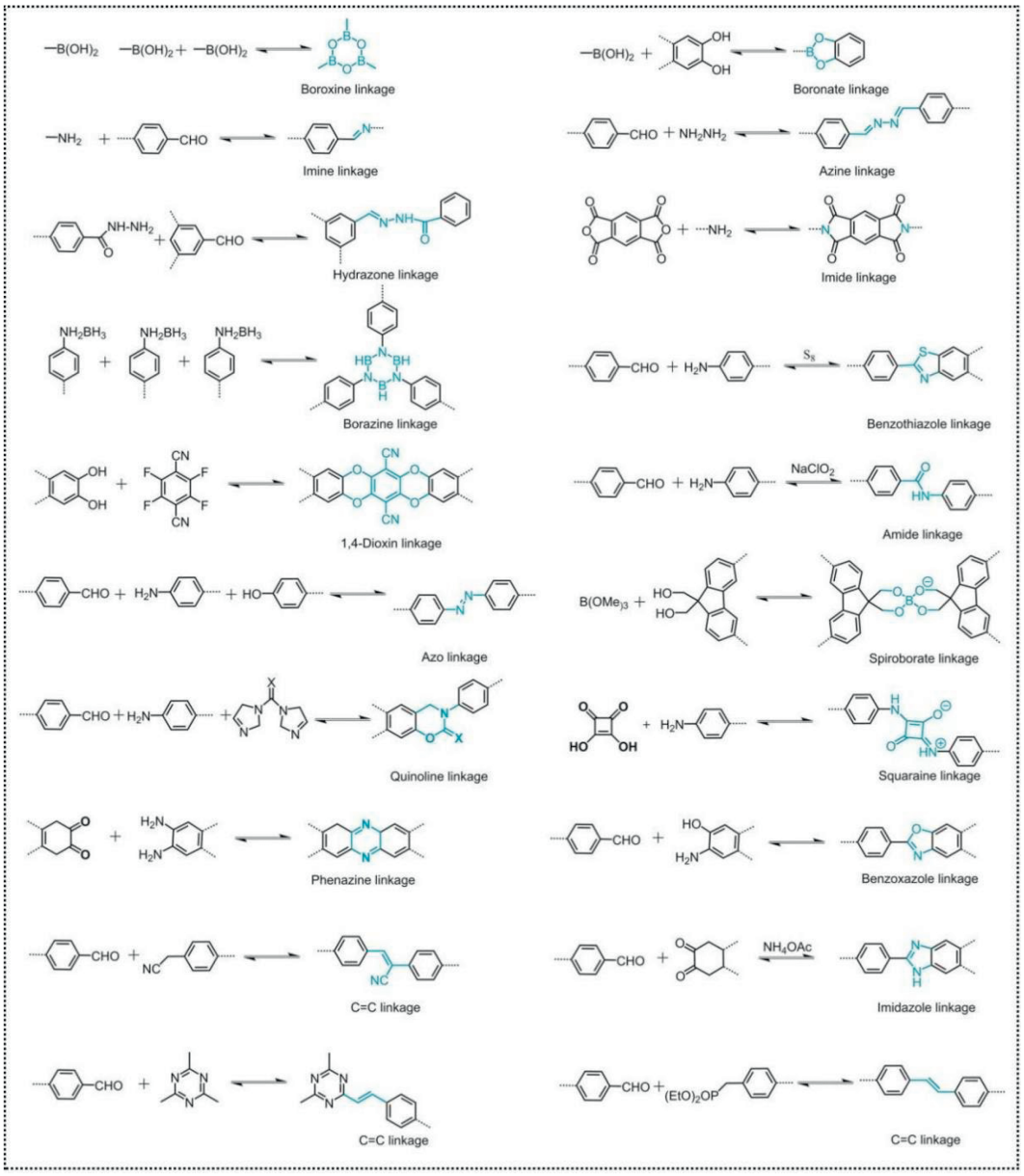


Fig. 14. The typical reactions types for COFs materials.

efficiency of COF-2CN are determined to be 6.8 % and 0.6 % respectively under visible-light irradiation, which is significantly higher than other organic polymer (Fig. 16e). COF-2CN also presents excellent photocatalytic stability in long time test (Fig. 16f). And the COF-2CN also showed the excellent stability in different pH (from 3 to 11), suggesting COF-2CN can be used in different pH conditions. Importantly, COF-2CN exhibits similar photocatalytic production rates of H_2O_2 in different water environment compare to ultrapure water conditions (Fig. 16g). Fs-TA spectroscopy reveals that photo-excited carriers generated by COF-2CN can be dissociated more efficiently compare to COF-0CN and COF-1CN owing to COF-2CN possess four channels for charge transfer. To better understand the mechanism of dicyano group in increasing the charge transfer channels, DFT calculations were carried out. The results suggest that dicyano-functional group as electron acceptor in COF-2CN can accept more photo-excited electrons comparing with other samples, which is contribute to the rapidly charge transfer and resulting in efficient ORR process. In the $2e^-$ WOR process, the energy barrier of rate-determining step of COF-2CN is apparent lower than that by COF-0CN and COF-1CN (Fig. 16h), which suggests that the introduction of dicyano groups into COFs can possess superior H_2O dehydrogenation property. In ORR process, COF-2CN still exhibits the same result further suggesting dicyano groups can enhance photocatalytic over H_2O_2 production rate (Fig. 16i). This work not only open a new way to synthesize COF-based photocatalyst for efficient overall H_2O_2 photosynthesis by introducing the dicyano groups into COFs, but also develops a new way for the practical application of organic photocatalysts in H_2O_2 photosynthesis. The PDOS demonstrates that the C 2p orbital contributed by valence band top and conduction band bottom of all COFs, confirming the well π-delocalization for all COFs. The results are beneficial for the efficient charge transfer of ORR process. In his work, author tests the photocatalytic activity using differentwater quality (such as tap water, river water, and lake water), which contribute to practical application. But this work is deficient in the sustainable production of H_2O_2. Chen's group report vinyl modified COFs (DVA-COF) for improving the photocatalytic H_2O_2 generation efficiency (Fig. 17a) [152].

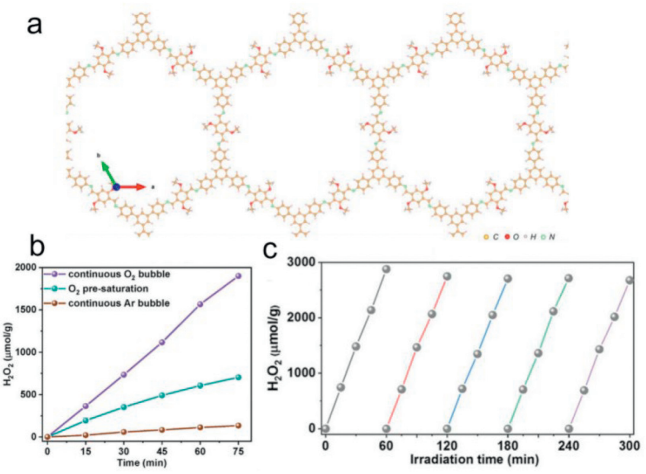


Fig. 15. (a) Structure model of TPB-DMTP-COF. (b) Visible light-driven H_2O_2 production in pure water. (c) Photocatalysis stability testing of TPB-DMTP-COF. Copied with permission [134]. Copyright 2021, Wiley-VCH GmbH.

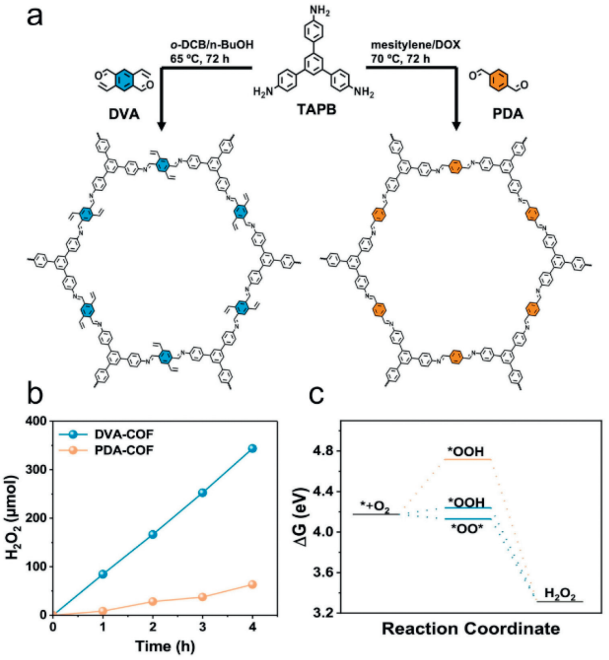


Fig. 17. (a) Synthetic routes used to prepare samples. (b) Photocatalytic performance curves over obtained samples. (c) Free energy diagram of ORR pathways for PDA-COF (orange) and DVA-COF (blue). Copied with permission [30]. Copyright 2024, Wiley-VCH GmbH.

This research suggested that the anchored vinyl groups in DVA-COF not only extended the light response range but also improve carrier separation and transfer efficiency that facilitate H_2O_2 production rate by a $2e^-$ ORR pathway. Therefore, DVA-COF with vinyl group produced H_2O_2 much more (84.5 μmol/h) than PDA-COF (8.6 μmol/h), which is also superior to most reported COFs-based photocatalysts (Fig. 17b). Moreover, DFT calculations showed that the introduction of vinyl groups improves the O_2 adsorption and affects the catalytic efficiencies, which decreases the barrier energy of O_2 adsorption affinity toward O_2, thereby optimizing the photocatalytic activity of DVA-COF (Fig. 17c). EPR characterization results suggest $^{\bullet}O_2^-$ is a significant intermediate in the photocatalytic overall H_2O_2 production process using PDA-COF. Additionally, Zhang *et al.* introduced kfto-form anthrahydroquinone into COFs (kf-AQ) by mechanochemical synthesis (Fig. 18a) [153]. Kfto-form anthraquinone containing COF showed efficient H_2O_2 photosynthesis in alkaline water, with a record H_2O_2 production rate of

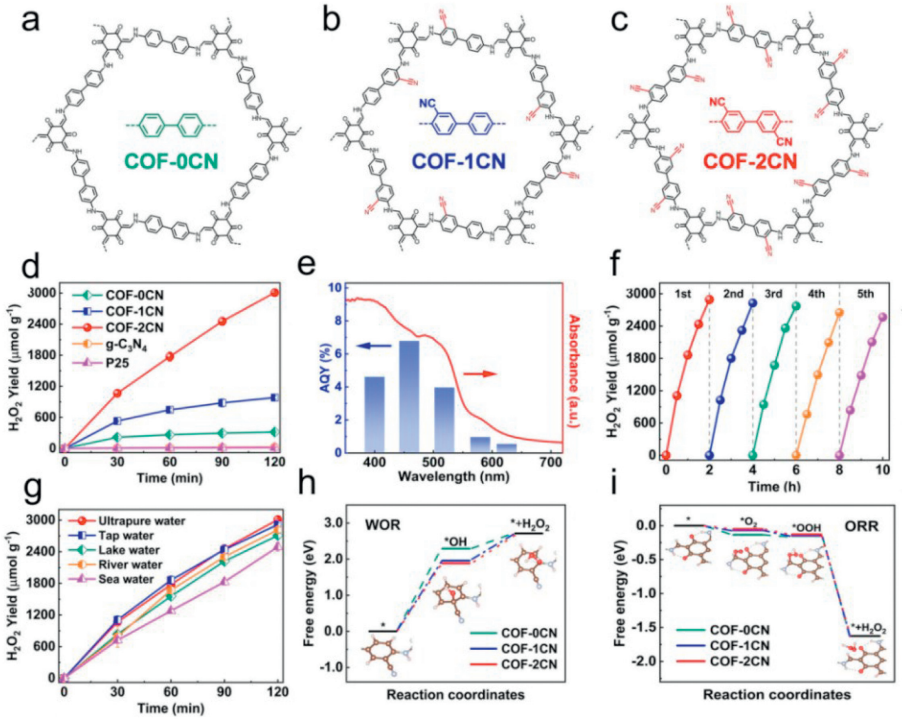


Fig. 16. Chemical structure of COF-0CN (a), COF-1CN (b) and COF-2CN (c). (d) Time-dependent H_2O_2 photogeneration using visible light for fabricated samples. (e) The AQY of COF-2CN at selected wavelength. (f) Long-term testing of COF-2CN for H_2O_2 photosynthesis. (g) Photocatalytic H_2O_2 production by COF-2CN in ultrapure water, tap water, river water, lake water and sea water under visible-light irradiation. Calculated energy profile for oxidation of water into H_2O_2 (h) and reduction of oxygen into H_2O_2 (i) on three COFs at $U = 0$ V *vs.* SHE at pH 7. Copied with permission [151]. Copyright 2024, Wiley-VCH GmbH.

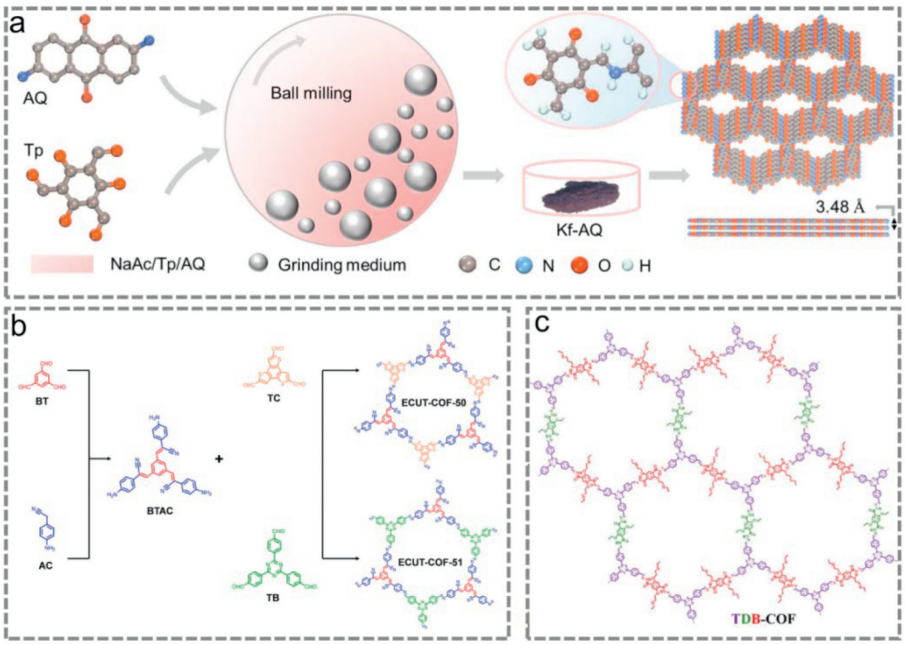


Fig. 18. (a) a Schematic of Kf-AQ condensation. Reprinted with permission [153]. Copyright 2024, Springer Nature. (b) The synthetic route of cyanide-functionalized D-A-π-D ECUT-COF-50 and D-A-π-A ECUT-COF-51. Reprinted with permission [154]. Copyright 2025, Elsevier. (c) Chemical structure of TDB-COF. Reprinted with permission [155]. Copyright 2023, Elsevier.

4784 μmol h^{-1} g^{-1} under visible light irradiation without reagents. The keto-form structure in Kf-AQ can enhance the water adsorption through the formation of OH^- clusters with weakened hydrogen bonds according to the dehydrogenation of water and efficient H_2O_2 photosynthesis. Luo *et al.* reported a COFs with cyanide group for highly efficient overall H_2O_2 generation from air and water through photocatalytic ORR and WOR (Fig. 18b) [154]. Without using any sacrificial agent, the synthesized COF is found to enable a H_2O_2 production rate as high as 4742 μmol h^{-1} g^{-1} from water and air and O_2 utilization and the SCC up to 0.68, which is bigger than most reported COFs and other organic photocatalysts. This study inspires a rational design of efficiency COF photocatalyst for high-performance artificial photocatalysis. Shen's group designed and developed thioether-decorated triazine-based COF (TDB-COF) for efficient overall H_2O_2 photosynthesis. TDB-COF exhibits an excellent photocatalytic H_2O_2 production rate of 723.5 μmol h^{-1} g^{-1} without any sacrificial agents and presents remarkable cyclic stability (Fig. 18c) [155]. The modification of thioether groups extended the light absorption range of TDB-COF and narrowed its energy band gap. Experimental and theoretical analysis revealed that this method can not only effectively optimize the band structure and improve visible-light absorption for $2e^-$ WOR but also enhance the photo-excited carriers transfer and separate for $2e^-$ ORR process to generate H_2O_2, thus resulting ultimately boosting the overall H_2O_2 photosynthesis. This work provides deeply suggestions for the development of the functional COFs towards overall H_2O_2 photosynthesis.

3.4.2. D-A structures

Enhancing the photocatalytic efficiencies necessitates a key stage of separation and rapid migration of photo-excited carriers. D-A structures offer several advantages for photosynthesis owing to the construction of internal electric field that facilitate carrier separation and transfer, also wide light response ranges, enabling them to absorb a broad zone of the solar spectrum [142,156–158]. In addition, D-A system can effectively reduce the exciton binding energy based on previous theoretical studies and experiments. The COFs with various D-A building blocks can be selected to meet O_2 reduction and water oxidation band structures and energy band requirements. Therefore, the energy levels of D—A materials can be customized for optimal alignment with the redox potentials of photocatalytic overall H_2O_2 production. Further, COFs with the large specific surface area and high porosity can offer more active sites for O_2 adsorption, subsequently increase the local O_2 concentration of catalyst surface, and capture photo-excited electrons. To explore these properties, Mou and co-workers reported three kinds of azoles-linked COFs including thiazole-linked TZ-COF, oxazole-linked OZ-COF and imidazole-linked IZ-COF for photocatalytic overall H_2O_2 generation (Fig. 19a) [143]. They demonstrated that electron-rich pyrene building block server as electron donor and the azole linkage acts as an acceptor leading to the electron directional transfers from pyrene block to azole fragments. Additionally, light absorption, energy levels and photo-excited carrier transfer can be modulated easily by constructing D-π-A structure. TZ-COF displayed the highest SCC value of 0.036 % and AQY of 0.6 % at 475 nm among all of them due to the more accessible channels of charge transfer were constructed in TZ-COF *via* the donor-π-acceptor structure. Fs-TA spectroscopy was carried out to study photoexcited carrier dynamics. And the results demonstrated TZ-COF has a longer-lived excited state absorption decay than OZ-COF and IZ-COF, which is agreement with the high efficiency of photoexcited carrier separation and transfer. DFT calculations and partial density of states (PDOS) were carried out (Fig. 19b). The computational results suggested that the benzene ring fragment between pyrene unit and azole linkage can absorb O_2 efficient by donor-acceptor complex reaction, which combine the photo-excited electrons to generate $^*O_2$. And it further integrates with the proton to generate $^*OOH$ intermediate for the formation of H_2O_2. Moreover, the O_2 can be generated by H_2O oxidation through photoinduced h^+, which is benefit to liberation O_2 for H_2O_2 generation under the condition of low or no O_2 concentration. Zhai *et al.* presented a mixed-linker strategy to construct a donor-acceptor-acceptor (D–A–A) type COF photocatalyst, FS-OHOMeCOF (Fig. 19c) [159]. The FS-OHOMe-COF structure characteristics widen π–π conjugation that enhances charge mobility,

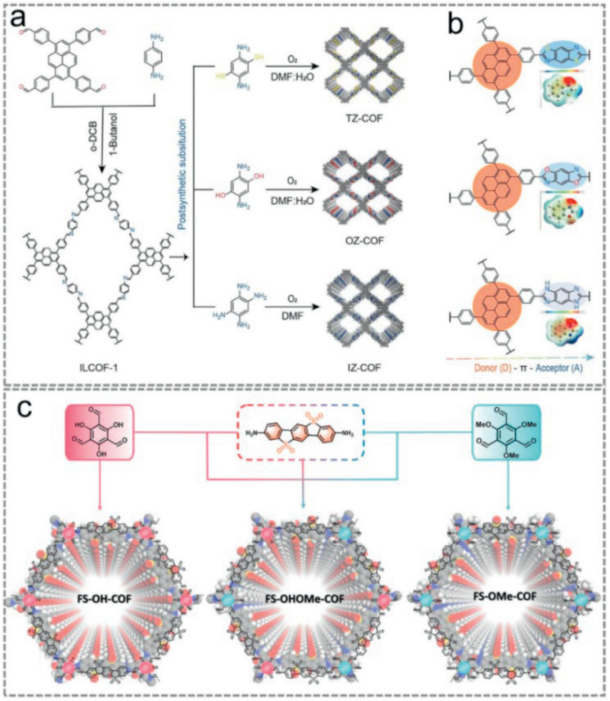


Fig. 19. Synthetic routes (a) of TZ-COF, OZ-COF and IZ-COF. (b) D-π-A model and differences of COFs (the inset is the local charge distribution). Copied with permission [143]. Copyright 2023, Wiley-VCH GmbH. (c)The synthetic routes and chemical structures of the different samples. Copied with permission [159]. Copyright 2024, Wiley-VCH GmbH.

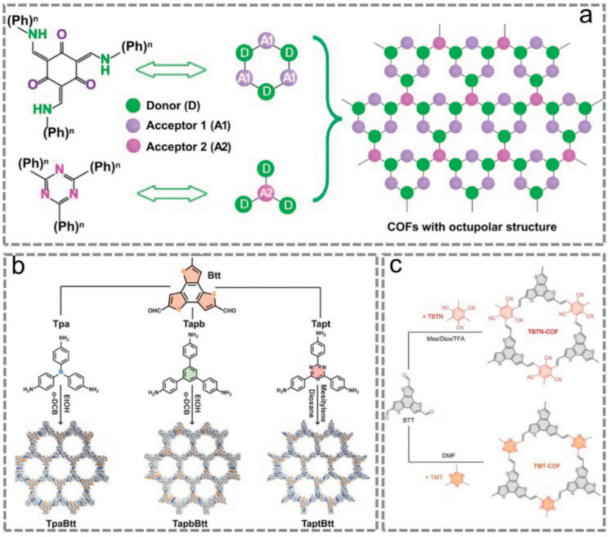


Fig. 20. The schematic illustration of the octupolar structure in different samples. Copied with permission [43]. Copyright 2023, Springer Nature. (b) Synthesis of TpaBtt, TapbBtt and TaptBtt. Copied with permission [137]. Copyright 2024, Springer Nature. (c) Synthetic routes of TBTN–COF and TMT-COF. Copied with permission [140]. Copyright 2024, Wiley-VCH GmbH.

while the introduction of sulfone groups not only as active sites facilitates the reactions rate between water and surface of catalyst but also increases stability through improved inter-layer forces. The test results of temperature-dependent PL spectroscopy demonstrated that electron donating TpOMe group in COFs can facilitate delocalized charge transfer. They investigated photocatalytic overall H_2O_2 generation for these samples, initially by suspending these COFs in pure water under visible light irradiation. The FS-OHOMe-COF possessed the highest overall H_2O_2 production rate than FS-OH–COF and FS-OMe-COF. The external quantum efficiency (EQE) and SCC was tested and determined to be 9.6% and 0.58%, which is higher than the most reported polymer photocatalysts. It was worth noting that the EQE and the SCC were superior to most metal-free photocatalysts ever reported which make it very appealing photocatalyst for photocatalytic overall H_2O_2 production. Liu *et al.* prepared another type of D-A COF with optimal intramolecular polarity by introducing phenyl functional groups as electron donors for modulating exciton separation and transfer to boost the direct photocatalytic overall H_2O_2 generation from water, air and sunlight (Fig. 20a) [43]. They find that weak intramolecular polarity in D-A COFs constrains excitons dissociation in D-A COFs was constrained by weak intramolecular polarity, yet excessive strong intramolecular polarity suppresses excitons formation and lowers photo-stability of COFs by weakened π-conjugated effect. The optimal intramolecular polarity in COFs (named COF-N32) can promote exciton formation and dissociation, resulting in the high and stable H_2O_2 yield with SCC efficiency of 0.31%, which is superior to solar-to-biomass efficiency by plants (~0.1%). Wang's group report benzotrithiophene (Btt)-based D-A COFs with spatially separated redox centers for the photocatalytic production of H_2O_2 from water and oxygen without any sacrificial agents (Fig. 20b) [142]. They revealed the concept of a uniport "atom spot-molecular area" by a D-A strategies in CTFs to directly elucidate the differences of the energy band levels, charge transfer direction, and O_2 adsorption. The photocatalytic overall H_2O_2 about higher than that of TpaBtt (252 μmol g^{-1} h^{-1}) and TapbBtt (557 μmol g^{-1} h^{-1}), also exceeded most of the previously reported metal-free photocatalysts. The efficiency of SCC was further tested under 1 sun illumination and measured to be 0.297%, which was larger than natural synthetic plants. Wang's group successfully synthesized cyanide-COFs (TBTN–COFs) including 2,4,6-trimethylbenzene-1,3,5-tricarbonitrile (TBTN) and benzotrithiophene-2,5,8-tricarbaldehyde (BTT) building blocks with water-affinity and charge-transfer (Fig. 20c) [160]. The TBTN–COF exhibits excellent overall H_2O_2 production with the highest H_2O_2 yield of 11,013 μmol g^{-1} h^{-1}, which was about double higher than that of TMT-COF (6392.3 μmol g^{-1} h^{-1}). The TBTN–COF shows a AQY value of 7.59% at 420 nm wavelength, which exceeded most reported COFs photocatalysts.

3.4.3. Heterojunction

COFs offer a diverse array of functional groups like hydroxyl, amino, and aldehyde for construction the heterojunction photocatalysts [161–163]. These groups, when combined with another semiconductor, can form stable heterojunctions photocatalysts that effectively separation electrons and holes. Huang's research group reported a heterostructure composed by covalent bonded COFs and perylene diimide polymers for photocatalytic overall H_2O_2 production from water and oxygen under visible light irradiation (Fig. 21a) [164]. Detail experimental and theoretical calculations analysis has revealed formation an interfacial electric field (IEF) between COFs and perylene diimide polymers, which creates an internal driving force to improve the separation rate of photo-excited electron and hole. Moreover, mechanistic studies suggest that the H_2O_2 generation accompany a simultaneous $2e^-$ ORR and $4e^-$ OER process. The photocatalytic overall H_2O_2 generation of the heterostructure has been tested in an O_2-saturated seawater. The H_2O_2 production is only 782, 641, and 996 μmol g^{-1} h^{-1} for single COFs and perylene diimide polymers, respectively. After formation the heterojunctions between COFs and perylene diimide polymers, the overall H_2O_2 production rate sharply raised to 3846 μmol g^{-1} h^{-1} with the suitable composition (Fig. 21b), suggesting the enhancement in photocatalytic overall H_2O_2 production rate owing to cre-

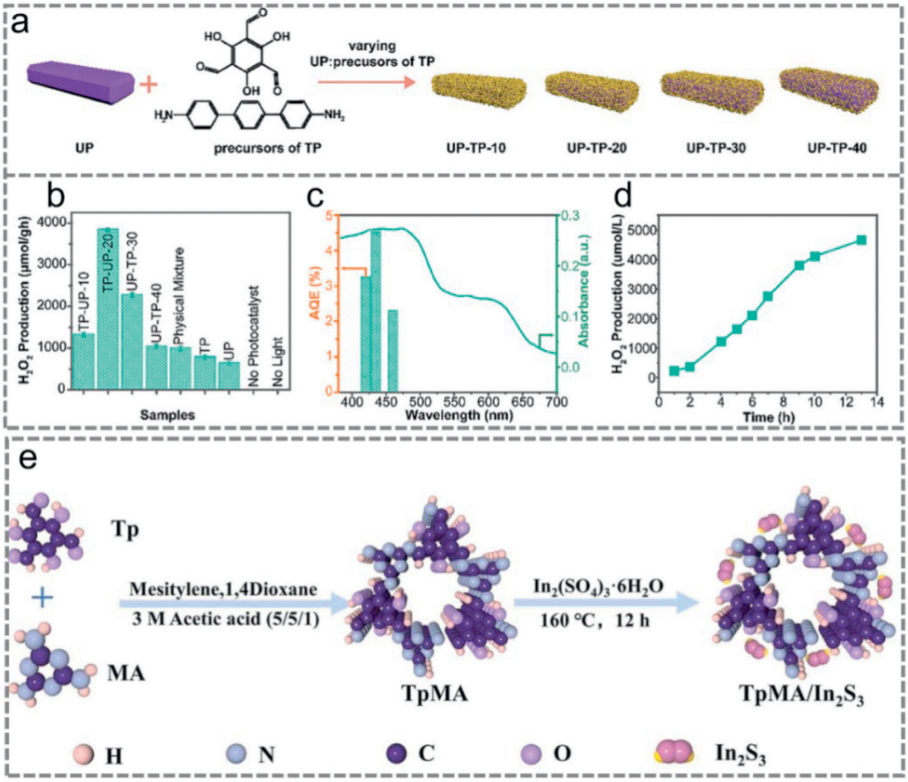


Fig. 21. (a) Schematic illustration the synthesis process of the UP-TP. (b) Photocatalytic overall H_2O_2 generation of various photocatalysts. (c) Wavelength-dependent AQE of H_2O_2 generation over UP-TP and the corresponding DRS spectrum. (d) Continuous H_2O_2 production over long-time testing. Copied with permission [164]. Copyright 2024, Wiley-VCH GmbH. (e) Schematic illustration of the synthesis process for TpMA/In_2S_3. Copied with permission [104]. Copyright 2024, Elsevier.

ation of IET. The AQE of heterostructure was tested and determined to be 3.24 %, 4.52 %, and 2.29 % at the wavelength of 420, 435, and 460 nm have in seawater, respectively (Fig. 21c). The SCC efficiency of heterostructure was measured to be 0.24 %, which is larger than the typical photosynthetic efficiency of plants. The heterostructure showed excellent photocatalytic stability with no obvious performance decay when it was continuously irradiated (Fig. 21d). This study provides a universal approach for rational design heterostructure to enhance the electron-hole separation rate and activity of catalytic centers simultaneously. Functional groups provided by COF can also form stable heterojunctions when combined with an inorganic semiconductor. Bi's group reported construction of heterojunctions by combing indium sulfide (In_2S_3) and COFs, namely TpMA, for photocatalytic overall H_2O_2 production (Fig. 21e) [104]. TpMA/In_2S_3 heterojunctions with different In_2S_3 loading amount were prepared *via* a hydrothermal method. The optical characteristics of samples were investigated in detailed by UV–vis DRS, electrochemical impedance spectroscopy (EIS) and photocurrent. The In_2S_3 showed decreased band gap of 1.97 V compared with TpMA (2.36 V). Therefore, the optical absorption properties of TpMA/In_2S_3 heterojunctions were accompanied by a red-shift in the absorption edge. This result suggests that the heterojunction could extend light absorption range. EIS and photocurrent results confirmed the heterojunctions strategy could apparently enhance the generation, separation and transportation of light-excited carriers. The single TpMA and In_2S_3 showed poorly activity, generating about 237.14 and 31.76 μmol/L H_2O_2, respectively. It is obvious that the heterojunction samples presented apparently higher activity than single samples. TpMA and heterojunctions showed decreased activity in dark or within an Argon atmosphere suggesting that O_2 is an important component in the photocatalytic overall H_2O_2 generation.

4. Outlook and perspective

The photocatalytic overall H_2O_2 generation from H_2O and O_2 under sunlight irradiation is a promising way to alleviate energy crisis and environmental pollution. This review systemically summarizes recent advances in photocatalytic overall H_2O_2 production using metal-free photocatalysts, including g-C_3N_4, COFs and CTFs. Additionally, we discuss the primary research strategies for enhancing overall H_2O_2 generation. Despite recent progress, the photocatalytic overall H_2O_2 generation performance remains low, with the highest reported SCC efficiency reaching only 1.41 %. The low photocatalytic activity can be attributed to the inherent drawbacks of metal-free photocatalysts, particularly their limited charge separation and transfer efficiency, insufficient thermodynamic driving force for water oxidation, and restricted visible-light absorption. To improve the efficiency of metal-free photocatalysts for overall H_2O_2 generation, the following key aspects should be addressed:

(1) Photoexcited charge separation and transfer serve as a crucial link between light absorption and surface redox reactions, significantly affecting SCC efficiency. Photogenerated charge carriers, including electrons and holes, must efficiently migrate to the photocatalyst surface to drive the WOR and ORR for H_2O_2 production. Metal-free photocatalysts typically generate Frenkel exciton with strong binding energies under light illumination, making charge separation relatively difficult. Therefore, reducing exciton binding energy is a promising strategy for improving carrier separation. Various approaches, including doping, heterojunction engineering, and the introduction of functional groups, have been explored to lower exciton binding energy in metal-free photocatalysts. Although these strategies have led to some reductions in exciton binding energy, the improvements

remain insufficient for achieving significantly higher SCC efficiency. Therefore, further efforts should focus on developing new molecular structures to better regulate exciton binding energy. Efficient charge transfer is equally important for improving overall H_2O_2 generation. Current strategies aimed at enhancing the transfer rate of charge transfer strategies, such as reducing migration distance and doped, still fail to satisfy the practical application. Compared to inorganic semiconductors, organic photocatalyst generally contain substantial defects that promote charge recombination and hinder carrier mobility. To fundamentally improve charge transport efficiency, it is essential to minimize intrinsic defects in metal-free photocatalysts. In this regard, the development of innovative synthesis strategies to reduce defect density is urgently needed to enhance the overall performance of photocatalytic H_2O_2 generation.

(2) Novel strategies should be developed to extend the light response range of metal-free photocatalysts. Light absorption is the first step in photocatalytic reactions, and is a prerequisite for achieving subsequent reactions of photocatalytic overall H_2O_2. To extend the light absorption range, only a few methods have been developed, such as doped and heterojunctions. However, these strategies remain ineffective in significantly improve light absorption. For metal-free materials, enhancing crystallinity and conjugation can generally enhance improve light absorption and charge transport within the skeleton, which is beneficial for increasing the efficiency of SCC conversion process. Additionally, other strategies, such as introducing electron donor groups and photosensitizer into metal-free photocatalysts, should also be explored. The effectiveness of these approaches in enhancing light absorption has already been demonstrated in previous studies.

(3) Compared to ORR progress, the WOR reaction requires a higher redox potential to overcome thermodynamics barrier. Therefore, the design and development of new metal-free photocatalysts with sufficient thermodynamic driving force is crucial for achieving efficient overall H_2O_2 production. Various strategies have been reported for regulating the WOR thermodynamic driving force in metal-free photocatalysts, including single-atom doped, introducing acetylene and leveraging topological effects. Among them, most methods primarily focus on direct $2e^-$ WOR, which is thermodynamically more favorable than 1 e^- WOR. However, the $1e^-$ WOR exhibits superior kinetics compared to the $2e^-$ WOR due to the larger potential difference between the reaction and photo-excited holes. Additionally, on the oxidation side, the $1e^-$ WOR can release more protons from H_2O, significantly enhancing the hydrogenation rate during the $2e^-$ ORR process. Therefore, a promising strategy for achieving highly efficient photocatalytic overall H_2O_2 generation is the development of new metal-free photocatalysts with an efficient $1e^-$ WOR capability. Here we could study carefully the effective strategy from electrocatalysis and thermal catalysis to improve the WOR thermodynamic driving force of photoctalysis.

(4) Machine learning (ML) is an important area of artificial intelligence that produces different models and resolves various challenging issues. The ML has been widely used in electrocatalysis to help researchers better understand the mechanism of electrocatalytic reactions. In recent years, ML techniques also develop rapidly in accelerating the synthesis and discovery of efficient photocatalysts for H_2O_2 generation. Training model to predict active solar photocatalysts with available knowledge could subsequently lead toward rationally synthesizable photocatalysts for overall H_2O_2 generation. The combination of ML and photocatalysis overall H_2O_2 production learning might pave the road toward open of efficient catalyst screening platform significant benefiting photocatalysis H_2O_2 generation community. Thus, given a basic description about photocatalysis overall H_2O_2 production, such as light harvesting, photoexcited separation and transfer, redox reaction, and training them to discovery of efficient photocatalysts is a future crucial research paradigm.

(5) The poor stability of metal-free photocatalysts should be carefully addressed. To improve the stability of metal-free photocatalysts, the robust chemical bond should be considered, such as polyimide and polyetherether. And the improvement the crystallinity of metal-free photocatalysts is an also effective strategy to enhance the stability. Another feasible method is protection mechanisms, such as coating protective layer at the surface of metal-free photocatalysts.

In summary, significant challenges remain, and substantial efforts are needed to overcome the low SCC efficiency in overall H_2O_2 generation. Nevertheless, metal-free photocatalysts remain promising materials for efficient, green and sustainable overall H_2O_2 generation due to their unique physical chemistry characteristics. In recent years, remarkable progress has been made, with metal-free photocatalysts achieving an SCC of up to 1.41 % for overall H_2O_2 production. It is therefore highly possible that the utilization of metal-free photocatalysts for overall H_2O_2 generation could help bridge the gap toward achieving industrial application.

Declaration of competing interest

The authors declare that they have no known competing financial interests or personal relationships that could have appeared to influence the work reported in this paper.

CRediT authorship contribution statement

Congxu Wang: Writing – original draft. **Xuan Xie:** Writing – original draft. **Feng Qiu:** Supervision. **Lei Zhu:** Writing – original draft. **Imran Shakir:** Writing – review & editing. **Yuxi Xu:** Supervision, Project administration.

Acknowledgments

This work was supported by the National Natural Science Foundation of China (No. 22409038, 52473221), Zhejiang Province Postdoctoral Science Foundation (No. ZJ2024021), Hubei Provincial Natural Science Foundation of China (Nos. 2024DJC032, 2025AFB889), Key Project of Science and Technology Research of Hubei Provincial Department of Education (Nos. D20232701, D20232702). I. Shakir acknowledges the research grant funded by the Research, Development, and Innovation Authority (RDIA) - Kingdom of Saudi Arabia (No. 12615-iu-2023-IU-R-2-1-EI-).

References

[1] Y.X. Fang, Y.D. Hou, X.Z. Fu, X.C. Wang, Chem. Rev. 122 (2022) 4204–4256.
[2] J. Quílez-Bermejo, S. García-Dalí, A. Daouli, et al., Adv. Funct. Mater. 33 (2023) 2300405.
[3] M.Z. Rahman, M.G. Kibria, C.B. Mullins, Chem. Soc. Rev. 49 (2020) 1887–1931.
[4] P.Y. Du, L. Yuan, T. Bao, et al., Chin. Chem. Lett. 36 (2025) 110472.
[5] M.Y. Qi, M. Conte, M. Anpo, Z.R. Tang, Y.J. Xu, Chem. Rev. 121 (2021) 13051–13085.
[6] Z.S. Huang, Y.F. Wang, M.Y. Qi, et al., Angew. Chem. Int. Ed. 63 (2024) e202412707.
[7] L.X. Zhang, Z.R. Tang, M.Y. Qi, Y.J. Xu, J. Mater. Chem. A 12 (2024) 19029–19038.
[8] H.J. Song, L.Y. Luo, S.Y. Wang, G. Zhang, B.J. Jiang, Chin. Chem. Lett. 35 (2024) 109347.
[9] X.H. Xu, Y. Sui, W.T. Chen, et al., Appl. Catal. B: Environ. 34 (2024) 123271.
[10] J.M. Li, N. Xu, Y.F. Zhang, H.J. Dong, C.M. Li, Chin. Chem. Lett. 36 (2025) 110470.
[11] L.Y. Qin, C.D. Ma, J. Zhang, T.H. Zhou, Adv. Funct. Mater. 34 (2024) 2401562.
[12] J.Y. Wang, J.J. Wang, S.J. Zuo, et al., Chin. Chem. Lett. 34 (2023) 108157.
[13] J. Cheng, Y.T. Wu, W. Zhang, et al., Adv. Mater. 37 (2024) 2410247.
[14] A. Alam, B. Kumbhakar, A. Chakraborty, et al., ACS Mater. Lett. 6 (2024) 2007–2049.

[15] Y.N. Zhang, C.S. Pan, G.M. Bian, et al., Nat. Energy 8 (2023) 361–371.
[16] Y. Luo, B.P. Zhang, C.C. Liu, et al., Angew. Chem. Int. Ed. 62 (2023) e202305355.
[17] J.N. Lu, J.J. Liu, L.Z. Dong, et al., Angew. Chem. Int. Ed. 62 (2023) e202308505.
[18] H.Z. Wang, C. Yang, F.S. Chen, G.F. Zheng, Q. Han, Angew. Chem. Int. Ed. 61 (2022) e202202328.
[19] M.P. Kou, Y.Y. Wang, Y.X. Xu, et al., Angew. Chem. Int. Ed. 61 (2022) e202200413.
[20] Y. Ding, S. Maitra, S. Halder, et al., Matter 5 (2022) 2119–2167.
[21] Z.Y. Teng, Q.T. Zhang, H.B. Yang, et al., Nat. Catal. 4 (2021) 374–384.
[22] H. Cheng, H.F. Lye, J. Cheng, et al., Adv. Mater. 34 (2021) e2107480.
[23] X.L. Chen, Y. Kondo, S.J. Li, et al., J. Mater. Chem. A 9 (2021) 26371–26380.
[24] L. Chen, C. Chen, Z. Yang, et al., Adv. Funct. Mater. 20 (2021) 2105731.
[25] H. Che, X. Gao, J. Chen, et al., Angew. Chem. Int. Ed. 60 (2021) 25546–25550.
[26] S. Wu, H.T. Yu, S. Chen, X. Quan, ACS Catal. 10 (2020) 14380–14389.
[27] J.X. Wang, J.C. Li, Z.N. Li, et al., Nano Res. 17 (2024) 5956–5964.
[28] S. Kou, S. Lian, X.D. Xie, et al., Nano Res. 17 (2024) 8036–8044.
[29] T. Liu, Z.H. Pan, J.J.M. Vequizo, et al., Nat. Commun. 13 (2022) 1034.
[30] L. Chen, L. Wang, Y.Y. Wan, et al., Adv. Mater. 32 (2019) 1904433.
[31] H.P. Peng, H.C. Yang, J.J. Han, et al., J. Am. Chem. Soc. 145 (2023) 27757–27766.
[32] C. Liu, T. Bao, L. Yuan, et al., Yu, Adv. Funct. Mater. 32 (2021) 2111404.
[33] R.M. Zhu, Y. Liu, W.K. Han, et al., Angew. Chem. Int. Ed. 64 (2025) e202412890.
[34] M.Q. Zhang, R.C. Liu, F.L. Zhang, et al., Colloid. Interface. Sci. 678 (2025) 1170–1180.
[35] J. Zhou, J.Y. Chen, N. Li, et al., Small 21 (2024) e2409006.
[36] C.S. Zhou, L. Tao, J. Gao, et al., J. Environ. Chem. Eng. 12 (2024) 113370.
[37] L. Zhang, C.X. Wang, Q.K. Jiang, P.B. Lyu, Y.X. Xu, J. Am. Chem. Soc. 146 (2024) 29943–29954.
[38] S.D. Wang, Z.P. Xie, D. Zhu, Nat. Commun. 14 (2023) 6891.
[39] W. Zhao, L. Luo, M.Y. Cong, et al., Nat. Commun. 15 (2024) 6482.
[40] Y.X. Liu, L. Li, Z.Y. Sang, et al., Nat. Synth. 4 (2024) 134–141.
[41] R.Y. Liu, Y.Z. Chen, H.D. Yu, et al., Nat. Catal. 7 (2024) 195–206.
[42] Y.Z. Chen, R.Y. Liu, Y.Y. Guo, et al., Nat. Synth. 3 (2024) 998–1010.
[43] F.Y. Liu, P. Zhou, Y.H. Hou, et al., Nat. Commun. 14 (2023) 4344.
[44] T.W. He, H.C. Tang, J. Wu, et al., Nat. Commun. 15 (2024) 7833.
[45] Y.B. Zhao, P. Zhang, Z.C. Yang, Nat. Commun. 12 (2021) 3701.
[46] W.J. Fan, B.Q. Zhang, X.Y. Wang, et al., Energy Environ. Sci. 13 (2020) 238–245.
[47] C.H. Chu, Q.H. Zhu, Z.H. Pan, et al., Proc. Natl. Acad. Sci. U. S. A. 117 (2020) 6376–6382.
[48] P. Ren, T. Zhang, N. Jain, et al., J. Am. Chem. Soc. 145 (2023) 16584–16596.
[49] Y. Shiraishi, M. Matsumoto, S. Ichikawa, S. Tanaka, T. Hirai, J. Am. Chem. Soc. 143 (2021) 12590–12599.
[50] L.J. Liu, M.Y. Gao, H.F. Yang, et al., J. Am. Chem. Soc. 143 (2021) 19287–19293.
[51] S. Zhao, X. Zhao, H. Zhang, J. Li, Y.F. Zhu, Nano Energy 35 (2017) 405–414.
[52] T. Yang, D. Zhang, A.G. Kong, et al., Angew. Chem. Int. Ed. 63 (2024) e202404077.
[53] Z.F. Li, Z.M. Dong, Z.B. Zhang, et al., Angew. Chem. Int. Ed. 64 (2025) e202420218.
[54] D.M. Tan, R. Zhuang, R.C. Chen, et al., Adv. Funct. Mater. 34 (2023) 2311655.
[55] Y. Yang, Q.Y. Guo, Q.W. Li, et al., Adv. Funct. Mater. 34 (2024) 2400612.
[56] X. Zhang, P.J. Ma, C. Wang, et al., Energy Environ. Sci. 15 (2022) 830–842.
[57] S.F. Feng, H. Cheng, F. Chen, et al., ACS Catal. 14 (2024) 7736–7745.
[58] Q. He, B. Viengkeo, X. Zhao, et al., Nano Res. 16 (2021) 1–7.
[59] S. Hu, Sustain. Energ. Fules 3 (2019) 101–114.
[60] Q.Q. Zhang, X. Chen, Z.S. Yang, et al., ACS Appl. Mater. Interfaces 14 (2022) 3970–3979.
[61] C.X. Wang, P.B. Lyu, Z. Chen, Y. Xu, J. Am. Chem. Soc. 145 (2023) 12745–12754.
[62] T. Sun, S. Li, L. Zhang, Y. Xu, Angew. Chem. Int. Ed. 62 (2023) e202301865.
[63] T. Sun, Y. Liang, Y. Xu, Angew. Chem. Int. Ed. 61 (2022) e202113926.
[64] J.Q. Li, W. Lyu, X.J. Mi, et al., Adv. Sci. 11 (2024) 2401966.
[65] X.J. Mi, J.Q. Li, W. Lyu, et al., Appl. Catal. B: Environ. 378 (2025) 125530.
[66] Q.R. Zeng, Z.H. Cheng, C. Yang, et al., Chin. J. Poly. Sci. 39 (2021) 1004–1012.
[67] W.S. He, J. Duan, H. Liu, et al., Prog. Polym. Sci. 148 (2024) 101770.
[68] W.W. Zhang, L.J. Chen, S. Dai, Nature 604 (2022) 72–79.
[69] M.D. Wang, P.H. Zhang, X. Liang, Nat. Sustain. 5 (2022) 518–526.
[70] Y.Z. Liu, Y.H. Ma, Y.B. Zhao, Science 351 (2016) 365–369.
[71] D.M. Zhao, Y.Q. Wang, C.L. Dong, Nat. Energy 6 (2021) 388–397.
[72] C.S. Diercks, O.M. Yaghi, Science 355 (2017) eaal1585.
[73] Y.W. Zeng, P. Gordiichuk, T. Ichihara, Nature 602 (2022) 91–95.
[74] X.D. Zhang, D.D. Gao, B.C. Zhu, et al., Nat. Commun. 15 (2024) 3212.
[75] J.R. Wang, K.P. Song, T.X. Luan, et al., Nat. Commun. 15 (2024) 1267.
[76] S.S. Chen, T. Takata, K. Domen, Nat. Rev. Mater. 2 (2017) 1–17.
[77] Z. Wang, C. Li, K. Domen, Chem. Soc. Rev. 48 (2019) 2109–2125.
[78] L. Wang, X.S. Zhang, L. Chen, Y.J. Xiong, H.X. Xu, Angew. Chem. Int. Ed. 57 (2018) 3454–3458.
[79] Q. Zhang, K.Y. Gu, C.R. Dong, et al., Angew. Chem. Int. Ed. 64 (2024) e202417591.
[80] J. Ma, C. Peng, X.X. Peng, et al., J. Am. Chem. Soc. 146 (2024) 21147–21159.
[81] B.Y. Zhai, H.G. Li, G.Y. Gao, et al., Adv. Funct. Mater. 32 (2022) 2207375.
[82] T. Mahvelati-Shamsabadi, H. Fattahimoghaddam, B.K. Lee, H. Ryu, J.I. Jang, Chem. Eng. J. 423 (2021) 130067.
[83] Y. Shiraishi, S. Kanazawa, Y. Kofuji, et al., Angew. Chem. Int. Ed. 53 (2014) 13454–13459.
[84] S. Samanta, R. Yadva, A. Kumar, A.K. Sinha, R. Srivastava, Appl. Catal. B: Environ. 259 (2019) 118054.
[85] Y.J. Zhao, Y. Liu, Z.Z. Wang, et al., Appl. Catal. B: Environ. 289 (2021) 120035.
[86] J.Z. Zhang, J.Y. Lang, Y. Wei, et al., Appl. Catal. B: Environ. 298 (2021) 120522.
[87] Y.X. Ye, C. Wen, J.H. Pan, et al., Appl. Catal. B: Environ. 285 (2021) 119726.
[88] C.C. Chu, W. Miao, Q.J. Li, et al., Chem. Eng. J. 428 (2022) 132531.
[89] T.S. Shan, J.S. Li, S.Y. Wu, et al., Chem. Eng. J. 478 (2023) 147509.
[90] X. Zhang, H. Su, P.X. Cui, et al., Nat. Commun. 14 (2023) 7115.
[91] H. Tan, P. Zhou, M.X. Liu, et al., Nat. Synth. 2 (2023) 557–563.
[92] Q.C. Chen, C.J. Lu, B.Y. Ping, et al., Appl. Catal. B: Environ. 324 (2023) 122216.
[93] J.X. Hou, K.W. Wang, X. Zhang, et al., ACS Catal. 14 (2024) 10893–10903.
[94] H.W. He, Z.L. Wang, J.F. Zhang, et al., Adv. Funct. Mater. 34 (2024) 2315426.
[95] Y. Shen, J.Q. Shi, Y.H. Wang, et al., Chem. Eng. J. 498 (2024) 155774.
[96] M. Fu, J.H. Luo, B. Shi, et al., Angew. Chem. Int. Ed. 63 (2024) e202316346.
[97] Y. Liu, W. Miao, Z. Chen, et al., Chem. Eng. J. 496 (2024) 153871.
[98] P.P. Sun, K. Zhong, X.H. Huang, et al., Appl. Catal. B: Environ. 366 (2025) 124998.
[99] L.F. Li, F. Ye, Q.R. Li, et al., Appl. Catal. B: Environ. 363 (2025) 124802.
[100] Z.H. Xue, D.Y. Luan, H.B. Zhang, X.W. Lou, Joule 6 (2022) 92–133.
[101] B. Yu, Y. Zhao, G. Li, et al., CCS Chem. 7 (2025) 3308–3319.
[102] Z.Y. Teng, H.B. Yang, Q.T. Zhang, et al., Nat. Chem. 16 (2024) 1250–1260.
[103] Y.P. Yang, Y. Li, X.Q. Ma, et al., Catal. Sci. Technol. 13 (2023) 5599–5609.
[104] H.Y. Chen, S.J. Gao, G.C. Huang, et al., Appl. Catal. B: Environ. 343 (2024) 123545.
[105] P. Bika, I. Papailias, T. Giannakopoulou, et al., Catalysts 13 (2023) 1331.
[106] Z.F. Qian, Z.J. Wang, K.A.I. Zhang, Chem. Mater. 33 (2021) 1909–1926.
[107] H.W. He, Z.L. Wang, J.F. Zhang, et al., Adv. Funct. Mater. 34 (2024) 2315426.
[108] C.X. Wang, H.L. Zhang, W.J. Luo, T. Sun, Y.X. Xu, Angew. Chem. Int. Ed. 60 (2021) 25381–25390.
[109] Z. Yang, H. Chen, S. Wang, et al., J. Am. Chem. Soc. 142 (2020) 6856–6860.
[110] P. Kuhn, M. Antonietti, A. Thomas, Angew. Chem. Int. Ed. 47 (2008) 3450–3453.
[111] S.J. Ren, M.J. Bojdys, R. Dawson, et al., Adv. Mater. 24 (2012) 2357–2361.
[112] L.Y. Li, W. Fang, P. Zhang, et al., J. Mater. Chem. A 4 (2016) 12402–12406.
[113] Z. Cheng, W. Fang, T.S. Zhao, et al., ACS Appl. Mater. Interfaces 10 (2018) 41415–41421.
[114] M.Y. Liu, Q. Huang, S.L. Wang, et al., Angew. Chem. Int. Ed. 57 (2018) 11968–11972.
[115] H. Duan, P. Lyu, J. Liu, Y. Zhao, Y. Xu, ACS Nano 13 (2019) 2473–2480.
[116] H. Wang, L.T. Shi, Z. Qu, et al., ACS Appl. Mater. Interfaces 16 (2024) 2296–2308.
[117] W.J. Zhang, Z.Z. Deng, J.Y. Deng, et al., J. Mater. Chem. A 10 (2022) 22419–22427.
[118] R.X. Sun, B.E. Tan, Chem. Res. Chin. U 38 (2022) 310–324.
[119] C.B. Wu, Z.Y. Teng, C. Yang, et al., Adv. Mater. 34 (2022) e2110266.
[120] H. Zhang, W.X. Wei, K. Chi, et al., ACS Catal. 14 (2024) 17654–17663.
[121] C. Zhu, Y.C. Yao, Q.L. Fang, et al., ACS Catal. 14 (2024) 2847–2858.
[122] S.S. Liu, C. Zhu, J.J. Xu, et al., Appl. Catal B: Environ. 344 (2024) 123629.
[123] A.P. Cote, A.I. Benin, N.W. Ockwig, et al., Science (1979) 310 (2005) 1166–1170.
[124] J.W. Colson, A.R. Woll, A. Mukherjee, et al., Science (1979) 332 (2011) 228–231.
[125] S. Lin, C.S. Diercks, Y.B. Zhang, et al., Science (1979) 349 (2015) 1208–1213.
[126] X.Y. Guan, H. Li, Y.C. Ma, et al., Nat. Chem. 11 (2019) 587–594.
[127] S. Bi, F.C. Meng, D.Q. Wu, F. Zhang, J. Am. Chem. Soc. 144 (2022) 3653–3659.
[128] Z.X. Zhang, S. Bi, F.C. Meng, et al., J. Am. Chem. Soc. 145 (2023) 16704–16710.
[129] X. Chi, Z.X. Zhang, M.Q. Li, et al., Angew. Chem. Int. Ed. 64 (2025) e202418895.
[130] J. Zhang, X. Fei, Z.G. Wang, Angew. Chem. Int. Ed. 64 (2025) e202425617.
[131] M.H. Liu, Y.C. Xu, Y.X. Liu, et al., Angew. Chem. Int. Ed. 64 (2025) e202505491.
[132] Y.H. Hou, F.Y. Liu, J.L. Liang, et al., Angew. Chem. Int. Ed. 64 (2025) e202505621.
[133] K. Yu, L. Gong, Z. Huang, Z. Yu, F. Luo, CCS Chem. 7 (2025) 2731–2741.
[134] L.J. Li, L.P. Xu, Z.F. Hu, J.C. Yu, Adv. Funct. Mater. 31 (2021) 2106120.
[135] L.C. Guo, Z.C. Huang, L.L. Gong, F. Luo, CCS Chem. 7 (2025) 3146–3159.
[136] H. Chen, H. Zhang, K. Chi, Y. Zhao, Nano Res. 17 (2024) 9498–9506.
[137] J.N. Chang, Q. Li, J.W. Shi, et al., Angew. Chem. Int. Ed. 62 (2023) e202218868.
[138] J.Y. Yue, L.P. Song, Y.F. Fan, et al., Angew. Chem. Int. Ed. 62 (2023) e202309624.
[139] D. Chen, W.B. Chen, Y.T. Wu, et al., Angew. Chem. Int. Ed. 62 (2023) e202217479.
[140] Q.B. Liao, Q.N. Sun, H.C. Xu, et al., Angew. Chem. Int. Ed. 62 (2023) e202310556.
[141] J.M. Sun, H.S. Jena, C. Krihnaraj, et al., Angew. Chem. Int. Ed. 62 (2023) e202216719.
[142] C. Qin, X. Wu, L. Tang, et al., Nat. Commun. 14 (2023) 5238.
[143] Y. Mou, X. Wu, C. Qin, et al., Angew. Chem. Int. Ed. 62 (2023) e202309480.
[144] J.Y. Yue, L.P. Song, Z.X. Pan, et al., ACS Catal. 14 (2024) 4728–4737.
[145] J.Y. Yue, J.X. Luo, Z.X. Pan, et al., Angew. Chem. Int. 63 (2024) e202405763.
[146] T. Xu, Z.Q. Wang, W.W. Zhang, et al., J. Am. Chem. Soc. 146 (2024) 20107–20115.
[147] S. Yang, Z. Gao, Z.Y. Hu, et al., Macromolecules 57 (2024) 2039–2047.
[148] X.Y. Wang, L.J. Chen, S.Y. Chong, Nat. Chem. 10 (2018) 1180–1189.
[149] R.F. Chen, Y. Wang, Y. Ma, et al., Nat. Commun. 12 (2021) 1354.
[150] C.Z. Li, J.L. Liu, H. Li, et al., Nat. Commun. 13 (2022) 2357.
[151] Y. Hou, P. Zhou, F. Liu, et al., Angew. Chem. Int. Ed. 63 (2024) e202318562.
[152] H. Yu, F.T. Zhang, Q. Chen, et al., Angew. Chem. Int. Ed. 63 (2024) e202402297.

[153] X.C. Zhang, S.L. Cheng, C. Chen, et al., Nat. Commun. 15 (2024) 2649.
[154] P.P. Sun, K. Zhong, X.H. Huang, et al., Appl. Catal B: Environ. 366 (2025) 124998.
[155] S.W. Guan, Z.H. Hou, J. Tan, et al., Appl. Catal B: Environ. 334 (2023) 122826.
[156] Y.M. Wang, H. Zhao, P.K. Li, et al., Chem. Eng. J. 491 (2024) 151825.
[157] M.J. Deng, L.Y. Wang, Z.L. Wen, et al., Green. Chem. 26 (2024) 3239–3248.
[158] R.C. Chen, C.M. Wu, L.H. Chung, et al., Chem. Mater. 36 (2024) 9928–9938.
[159] C. Shu, X.J. Yang, L.J. Liu, et al., Angew. Chem. Int. Ed. 63 (2024) e202403926.
[160] E.B. Zhou, F.T. Wang, X. Zhang, Y.D. Hui, Y.B. Wang, Angew. Chem. Int. Ed. 63 (2024) e202400999.
[161] Z.P. Li, T.Q. Deng, S. Ma, et al., J. Am. Chem. Soc. 15 (2023) 8364–8374.
[162] Z. Shan, M.M. Wu, D. Y, et al., J. Am. Chem. Soc. 144 (2022) 5728–5733.
[163] L.X. Li, Q.B. Yun, C.Z. Zhu, et al., J. Am. Chem. Soc. 144 (2022) 6475–6482.
[164] X.Y. Shi, Y. You, L. Huang, et al., Adv. Funct. Mater. 2024 (2023) 202414755.